Large displacements of slender beams in plane: Analytical solution by means of a new hypergeometric function

Christian Iandiorio, Pietro Salvini

Large Displacements of Slender Beams in plane: Analytical Solution by means of a new Hypergeometric function

AUTHORS: Christian Iandiorio - c.iandiorio@live.it

Pietro Salvini - Corresponding Author: salvini@uniroma2.it

AFFILIATIONS: Department of Enterprise Engineering University of Rome "Tor Vergata", Via del Politecnico 1, 00133 Rome , EU, Italy

Abstract

The goal of this paper is to present an analytical solution for large planar displacements of cantilever beams, avoiding the integration of elliptic integrals. The proposed solution takes advantage of a new hypergeometric function of two variables by which it is possible to obtain the parametric solution of the beam displacement. The solution concerns a cantilever beam subjected to an inclined force and a moment applied at the free end; nevertheless, it is easy to extend it to the case of multiple loads applied in intermediate positions of the beam. The beams have a constant section and initial curvature, the material is elastic, isotropic and homogeneous. It is shown how to extend the results to spring-hinged cantilever or simply supported beams, to loads attached to the beam axis (following forces), or to a cantilever beam having the unsupported end displaced by a rigid cable.

Various technical design curves are also provided; these allow an easy and fast estimate of the endpoint displacements.

Particular attention is given to the study of the convergence region and speed of this new hypergeometric function. The configurations examined, the methodologies and the procedures to carry on these solutions are explained in detail within the paper. Some comparisons with numerical results support the solution proposed.

Keywords

Large Displacement Beams; Analytical solution; Geometric non-linearity; Hypergeometric Functions

1. Introduction

The origin of the problem is often brought back to Euler, but it has far more distant origins.

Leonardo Da Vinci was probably the first scientist to empirically investigate the stress and strain distribution of beams subjected to bending (1493), he was followed by Galileo who studied the material response of cantilever beams (1638). Fundamental contributions are the publications regarding the material elasticity by Hooke [1] and the study of curvature of Newton "*Method of Fluxions and Infinite Series with its Applications to the Geometry of Curve-Lines* (1671)". Important contributions also belong to Leibniz and C. Huygens. The first researcher able to combine the material elasticity with the mathematical description of the curvature was James Bernoulli who, after years of research, conceptually linked the two aspects introducing the hypothesis of a linear relation between moment and curvature. In 1691, he generally discusses the *Elastica* problem, and in 1694 he publishes a first solution for beams subjected to large displacements. Many years later, Daniel Bernoulli, grandson of James, suggested Euler that the generalized problem of Elastica could be solved by a variational approach, that he was studying at that time. In 1744 Euler publishes "*Methodus inveniendi lineas curvas maximi minimive proprietate gaudentes, sive solutio problematis isoperimetrici lattissimo sensu accepti*". In the book's appendix he reported the generalized Elastica problem; he found and classified nine type of equilibrium curve expressed by integrals, unsolvable through standard functions. Some particular cases can be solved by series expansion [2], and he introduced the formula known as "Euler's critic load".

Many other scientists worked on *Elastica* problem with experimental approaches, among them A.J.C.B. Duleau and P.van Musschenbroek, who first proposed a critic load formula (1729), before Euler, the result was however not correct.

Considerably important was the Laplace's work [3], who in 1770 proposed the general equation of buckling load (whose first mode is Euler's critical load), through the linearization of Elastica's equation, expressed in intrinsic geometry (arch-length approach).

The breakthrough comes with L. Saalschütz, who in 1880 [4] solves the Elastica differential equations expressing curvature as a function of curvilinear abscissa, making use of Legendre elliptic integrals (for more historical information see [5], [6], [7]).

A modern setting and solution of large deflections of cantilever beams loaded at the end is due to Barten [8] (1944) and Bisshop and Drucker [9] (1945). They solve the problem with an approach similar to Saalschütz's; they exploited first and second complete and incomplete elliptic integrals, specifying the limit value of Cartesian coordinates of the beam, and providing graphic illustrations.

Since then, many others worked in similar ways; recent works based on analytical solutions are, for example, in [10], [11], [12].

Many numerical or computing techniques have been studied to approach the large displacement problem. The most used are the coupling of Runge-Kutta and non-linear shooting method ([13], [14]). In fact, the two boundary conditions are not expressed in the same initial point, but in the extremal points of the beam. This implies that the R.K. method, after its application, must be accompanied to an attempt method (hence the name "shooting") which involves solving for each configuration a non-linear system. A similar technique is used in [15], with the difference that the shooting method is replaced with Gauss-Legendre quadrature scheme.

Another remarkable method, belonging to the class of analytical-numerical type, is the Automatic Taylor expansion technique (ATET) [16]. This consists developing in Taylor series the unknown variable of the non-linear differential equation; then it requires to compute every constant of the serial development. This method has the advantage to obtain an approximated analytical solution, which can be further manipulated; however, the technique is computationally time-consuming, already after the first terms of the series.

It is straightforward that numerical methods offer a worthy approach when the differential equations, especially if non-linear, are difficult to manipulate through analytical procedures; but they suffer a significant computational cost, already for the simplest problems.

For these above-mentioned reasons, this paper proposes an alternative closed-form solution for the finite rotation (large displacements) problem of a planar elastic cantilever beam, loaded at its end. The present solution is, as we will see later on, very suitable to apply for the facing of more complex problems and compliant constraints. The resolution of even further configurations is possible but will not be exposed in the present paper. Hypergeometric series present the advantage of an easy analytical manipulation and the capability to represent any special function; furthermore, they offer an easy computer implementation. This

approach has already been widely used in various fields of engineering, including structural mechanics (for example to solve generalized equation of discs rotating at high speed with variable thickness and subjected to thermal gradient vs radius), and physics, mainly for non-relativistic quantum physics.

One of the most important advantages connected to the easy manipulation of hypergeometric series is that the uniform convergence region can be estimated. Furthermore, thanks to the analytical approach, it is possible to obtain the response (displacement, stress, strain) of only one point of the structure, unlike the requirements of the numerical methods, thus avoiding the need to integrate throughout the full length of the beam.

The analytical solution that we propose represents a different approach by respect to elliptic integrals, which aims at a rapid computation of the quantities of interest. The evaluation of elliptic integrals is still a very broad and discussed topic of research [17]. The methods of integration and therefore the research in the sector are divided into two categories. The first one has a more analytical nature being based on the Taylor expansion series [18].The second one is more purely numeric and is based on weighted numerical approximation as Gauss quadrature or on more specific methods such as double exponential or *tanh-sinh* quadrature methods [19]. These last are particular efficient when there is a point of singularity in the integral, as in the cases that will be examined later.

A common way to analytically calculate the complete elliptic integrals is to include them in their analytical representation in Gaussian hypergeometric series; hence the idea to use the connection between elliptic integrals and hypergeometric series. However, the solution of the exact bending (finite rotations) of a cantilever beam involves the use of incomplete elliptic integrals, which can be represented by the hypergeometric double series of Kampé de Fériet. Our solution involves the introduction of a new hypergeometric series. Our new hypergeometric series does not apply on the elliptic integrals but it faces directly the integration of the Elastica problem.

Comparing with the analytical representation by series of elliptic integrals, the main advantage of our approach lies in a fewer number of series required. This last consideration, together with the high speed of calculation of the hypergeometric series due to their recursive properties, provides an advantageous computational tool having a solid analytical basis that opens to incremental precision. The last can be further

increased, without losing any previous computational expenditure, which is not possible with classical numerical integration methods.

The advantages become even more evident when some inflection points are present in the final configuration, since an increasing number of integrals appear.

Given the isostatic constraint conditions here considered and the type of loads always in favour of curvature, in the present work inflection points are not possible.

It is mandatory to specify that the analytical solution is possible only if the initial curvature of the beam is constant, the material is homogeneous and isotropic, and its elastic response keeps linear. In this paper, the shear effect and the axial deformation are neglected on purpose, as they have a very small influence in slender beams. For more information on a complete theory, including shear effects and axial strains see [20], and for its solutions by means of elliptical integrals see [21].

The fields of typical applications of large displacement analysis (geometric non-linearity) are various, mainly related to precision and compliant mechanics. Compliant mechanisms are used for transmitting large movements, in an analogy with mechanisms presenting almost rigid bodies connected by hinges, prismatic pairs, etc. A recent application of the large displacement theory for compliant mechanisms is given in [22] concerning the adoption of semi-circular beams that behave like hinges in compliant mechanisms. Several applications regard soft robots, medical or surgery instruments, flexible electronics or in general MEMS (Micro-Electro-Mechanical Systems) ([23], [24]).

Besides the analytical details present in the paper, in paragraph 5 dimensionless curves are shown, which by entering the length of the beam, flexural stiffness and the angle of load, it is possible to obtain the end (load) point displacements and rotation without the computer aid. The curves regard both conservative loads (constant direction) and non-conservative loads (follower load).

2. Mathematical Background

In this section, we propose a new hypergeometric function, never mentioned before in literature according to the authors. This definition allows dealing with all the solutions required by means of a unique hypergeometric form. The range of the uniform convergence region is also determined. Concerning speed

convergence, this is discussed in the fourth section, where the truncation of the series is investigated through a tolerance criterion.

For the reader convenience, the integral representation of the hypergeometric series is also provided and developed in the appendix.

2.1 Definition of a new Hypergeometric function

The hypergeometric function accounted here assumes the form:

$$ {}^{\gamma}_{\beta}\mathrm{I}\left(\begin{matrix} a\,,\ b_1\ ,b_2 \\ \\ c_1\,,c_2 \end{matrix}\ ;\ x,y\right)=\sum_{n=0}^{\infty}\sum_{k=0}^{\infty}\frac{(a)_{\beta+\gamma n+k}\,(b_1)_n\,(b_2)_k}{(c_1)_{\beta+\gamma n}\,(c_2)_k}\,\frac{x^n\,y^k}{n!\,k!} $$

with: $\beta\,,\gamma\,,a\,,\ b_1\ ,b_2,c_1\,,c_2\ \in\mathbb{R}$

$(a)_m=a(a+1)(a+2)\ldots\ (a+m-1)$ is a rising factorial (Pochhammer symbol).

It is important to observe that, being $\beta\,,\gamma\in\mathbb{R}$, in this case the coefficient $m\in\mathbb{R}$, then the rising factorial cannot be calculated by the previous definition, but introducing the Euler Gamma function $\Gamma(\cdot)$ as:

$$(a)_m=\frac{\Gamma(a+m)}{\Gamma(a)}$$

If $a+m<0$ it is possible to extend the Pochhammer symbol-Gamma function relation for negative indices if and only if $(a+m)\in\mathbb{C}\backslash\{\mathbb{Z}^-,0\}$ (out of this region the rising factorial is not defined), using the relation:

$$\Gamma(-x)=-\frac{\pi}{x\,\Gamma(x)\sin(\pi x)}\qquad\forall\,x\in\mathbb{C}\backslash\{\mathbb{Z}^-,0\}$$

2.2 Some important properties recalled within the paper

We recall some important properties of the Pochhammer symbol and generalized binomial expansion, which will be useful in all the demonstrations that will be seen later.

1. $(a)_n=\frac{\Gamma(a+n)}{\Gamma(a)}$
2. $\Gamma(n)=(n-1)!$
3. $(a)_n(a-k)_k=(a-k)_{n+k}$
4. dimidiation formula: $(a)_n=\frac{(2a)_{2n}}{2^n\left(a+\frac{1}{2}\right)_n}$

5. $(a)_n = (-1)^n \binom{-a}{n} n!$

6. $(a+n)! = (a)!\,(a+1)_n$

7. $(a)_n = (a)_k (a+k)_{n-k}$

8. $\frac{1}{a \cdot n+1} = \frac{\left(\frac{1}{a}\right)_n}{\left(1+\frac{1}{a}\right)_n}$

9. Generalized Binomial expansion : $(x_1 + x_2)^\alpha = \sum_{n=0}^{\infty} (-1)^n \frac{(-\alpha)_n}{n!} {x_1}^{\alpha-n} {x_2}^n$, $|x_1| > |x_2|$

2.3 Uniform convergence region

The uniform convergence region of the hypergeometric series ${}^{\gamma}_{\beta}\mathrm{I}\left(\begin{matrix} a\,,\, b_1\,,\, b_2 \\ c_1\,,\, c_2 \end{matrix}; x, y\right)$ is given by:

$$|x|^{\frac{1}{\gamma}} + |y| < 1$$

Demonstration:

It is known that the region of convergence of a hypergeometric series is not affected by the values of Pochhammer symbols, in this case $a\,,\ b_1\ ,b_2, c_1\ , c_2$. For that reason it is possible to study the uniform convergence on a simpler equivalent series, with $a\,,\ b_1\ ,b_2, c_1\ , c_2 = 1$.

In the foregoing derivations, some of the previous properties used are marked with their number; as an example, if property 1 is used, the equality symbols is so enriched "$\overset{\{1\}}{=}$".

$${}^{\gamma}_{\beta}\mathrm{I}\left(\begin{matrix} 1\,,\, 1\,,\, 1 \\ 1\,,\, 1 \end{matrix}; x, y\right) = \sum_{n=0}^{\infty}\sum_{k=0}^{\infty} \frac{(1)_{\beta+\gamma n+k}\,(1)_n\,(1)_k}{(1)_{\beta+\gamma n}\,(1)_k} \frac{x^n\, y^k}{n!\, k!} \leq$$

$$\leq \sum_{n=0}^{\infty}\sum_{k=0}^{\infty} \frac{(1)_{\beta+\gamma n+k}\,(1)_n\,(1)_k}{(1)_{\beta+\gamma n}\,(1)_k} \frac{|x|^n\,|y|^k}{n!\, k!} \overset{\{1,2\}}{=} \sum_{n=0}^{\infty}\sum_{k=0}^{\infty} \frac{(\beta+\gamma n+k)!}{(\beta+\gamma n)!\ k!}\,|x|^n\,|y|^k \overset{\{6\}}{=}$$

$$= \sum_{n=0}^{\infty}\sum_{k=0}^{\infty} \frac{(\beta+\gamma n+1)_k}{k!}\,|x|^n\,|y|^k = \sum_{n=0}^{\infty} |x|^n \sum_{k=0}^{\infty} (\beta+\gamma n+1)_k \frac{|y|^k}{k!} \overset{\{9\}}{=}$$

$$= \frac{1}{1-|y|^{1+\beta}} \sum_{n=0}^{\infty} \left[\frac{|x|}{(1-|y|)^\gamma}\right]^n$$

The latter is a power series that uniform converges if and only if its argument is < 1, which confirm the thesis.

2.4 Integral representation

A useful property of hypergeometric function is its integral representation. This last could be convenient if the user does not want to compute the series in the classic way, as carried on in the foregoing section 4.

The general integral representation of the hypergeometric function, with $c_1 \neq a$, $c_2 \neq b_2$ is:

$$ {}_{\beta}^{\gamma}\mathrm{I}\left(\begin{matrix} a\,,\ b_1\ ,b_2 \\ c_1\,,c_2 \end{matrix};\ x,y\right) = $$

$$ = \frac{\Gamma(c_1)\,\Gamma(c_2)}{\Gamma(a)\,\Gamma(b_2)\,\Gamma(c_1-a)\,\Gamma(c_2-b_2)} \int_0^1 \int_0^1 t^{b_2-1}\,(1-t)^{c_2-b_2-1}\,u^{a+\beta-1}(1-u)^{c_1-a-1}(1-yt)^{-a-\beta}\left[1-x\left(\frac{u}{1-yt}\right)^{\gamma}\right]^{-b_1} du\,dt $$

However, in the solutions that will be proposed $c_1 = a$; this implies that the integral representation simplifies into:

$$ {}_{\beta}^{\gamma}\mathrm{I}\left(\begin{matrix} a\,,\ b_1\ ,b_2 \\ c_1\,,c_2 \end{matrix};\ x,y\right) = \frac{\Gamma(c_2)}{\Gamma(b_2)\Gamma(c_2-b_2)} \int_0^1 t^{b_2-1}\ (1-t)^{c_2-b_2-1}(1-yt)^{-a-\beta}\left[1-\frac{x}{(1-yt)^{\gamma}}\right]^{-b_1} dt $$

which is considerably simpler than the previous one.

The demonstration of how it is possible to obtain the integral representation, from the hypergeometric series, is proposed in the Appendix.

3. Elastica Solution

3.1 Differential equation concerning static equilibrium

Consider a beam with constant section and an initial unique value of curvature, subjected to concentrated forces and a moment applied at the free end (Fig.1). Under the hypothesis that one of the principal axis of the section lies in the plane *x*-*y*, both deformed and undeformed configurations develop in the same plane. The beam is slender, consequently, it behaves as inextensible; shear effects are negligible if compared to bending deformation and stresses/strains change linearly within the section. The material constituting the beam is linear elastic, homogeneous and isotropic.

Being *s* the curvilinear abscissa, $\psi_{in}(s)$ the angle giving the initial tangent direction at any point by respect to the *x*-axis, $\psi(s)$ the final angle of rotation, F and M the ending loads, the differential equation giving the static equilibrium of the cantilever beams in Fig.1, is:

$$EI\,\frac{d^2\psi}{ds^2} \pm F_x\,sin(\psi) + F_y\,cos(\psi) = 0 \qquad (1)$$

Where F_x is the projection of F in the x direction; it is considered positive if concordant with the positive direction of x-axis (*positive configuration*), negative otherwise (*negative configuration*); F_y is the projection of F in y-direction. E is the Young's module and I the moment of inertia of the section. As discussed hereinafter, the solutions follow different paths according to *positive* or *negative* configurations.

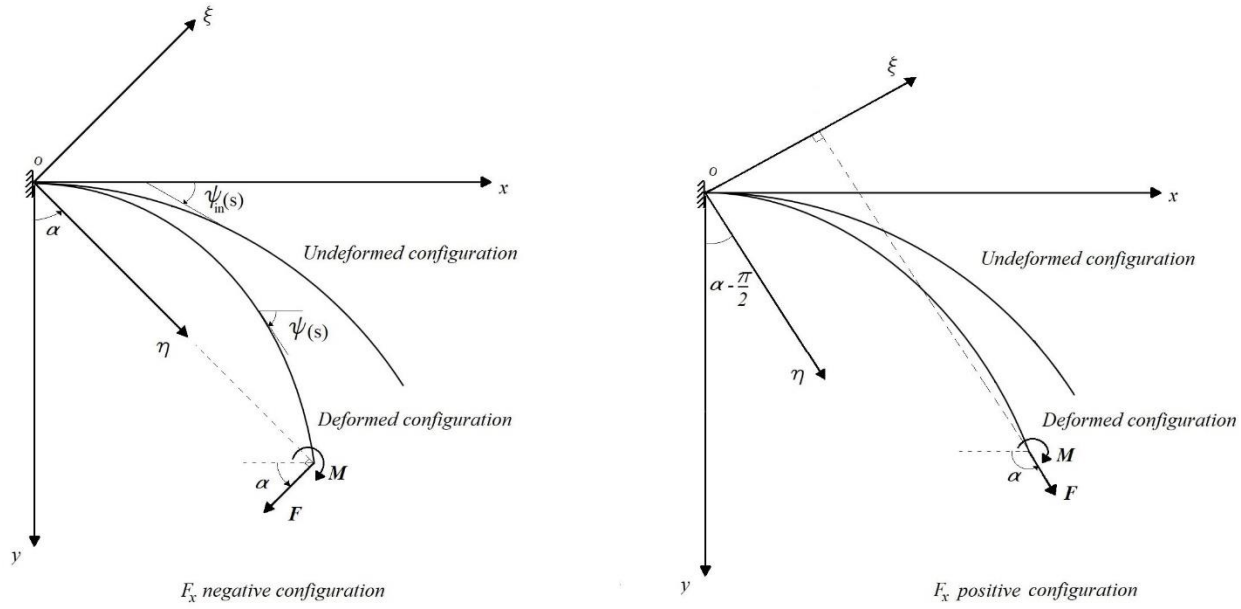

(a) (b)

Fig. 1. Beam in the F_x negative configuration (a), and F_x positive configuration (b)

Others important definitions are:

$k = \frac{d\psi}{ds}$ is the curvature of the beam when deformed

$k_{in} = \frac{d\psi_{in}}{ds}$ is the initial curvature of the beam

$k(s) - k_{in}(s) = \frac{\mathrm{M(s)}}{EI}$ is the Moment-curvature relationship (2)

Cardinal equations of intrinsic geometry:

$$dx = cos\,\psi\,ds$$

$$dy = sin\,\psi\,ds$$

For the complete discussion of how the generalized differential equation of static equilibrium is derived, if distributed loads also exist and the initial curvature of the beam is not constant, see [25].

3.2 Solution for F_x negative configuration

This configuration is verified for $0 \leq \alpha < \frac{\pi}{2}$ - Fig.1.(a).

Using simple trigonometric manipulations eq. (1) becomes:

$$\frac{d^2\psi}{ds^2} + \left(\frac{F}{EI}\right)\sin(\psi + \alpha) = 0 \tag{3}$$

For convenience, we turn the reference system for an α angle clockwise, switching to (O, ξ, η) system. This choice is essential for requiring only one function series evaluation for the two displacement components. The new reference respects the following cardinal equations:

$$\begin{aligned} \vartheta(s) &= \psi(s) + \alpha \\ \frac{d\xi}{ds} &= cos(\vartheta) \\ \frac{d\eta}{ds} &= sin(\vartheta) \end{aligned} \tag{4}$$

The previous equation (3) turns into:

$$\frac{d^2\vartheta}{ds^2} + \left(\frac{F}{EI}\right)\sin(\vartheta) = 0 \tag{5}$$

Using the substitution $\frac{d\vartheta}{ds} = Z(\vartheta)$:

$$Z\frac{dZ}{d\vartheta} + \left(\frac{F}{EI}\right) sin(\vartheta) = 0$$

The previous equation allows variable separation to integrate once, thus obtaining:

$$\frac{1}{2}\left(\frac{d\vartheta}{ds}\right)^2 - \left(\frac{F}{EI}\right) cos(\vartheta) + c_1 = 0$$

The integration constant of this equation is derived through the application of eq.(2) at the free end, (specified by an *L* at the subscript) as $\vartheta'_L = \psi'_L = k_{in} + \frac{M}{EI}$

$$ds = \frac{d\vartheta}{\sqrt{\left(\frac{2F}{EI}\right)\left[cos(\vartheta) - cos(\vartheta_L)\right] + \left(k_{in} + \frac{M}{EI}\right)^2}} \tag{6}$$

Now it remains to express the parametric equations of the beam by respect to (O, ξ, η) reference. Using the first and the last equation of (4) and (6) and imposing zero displacement at the constraint:

$$\eta(\psi) = \int_{\alpha}^{\psi+\alpha} \frac{\sin(\vartheta)}{\sqrt{\left(\frac{2F}{EI}\right)[cos(\vartheta) - cos(\psi_L + \alpha)] + \left(k_{in} + \frac{M}{EI}\right)^2}}\, d\vartheta \tag{7}$$

This last is an Abelian's integral, easy to solve analytically:

$$\eta(\psi) = \sqrt{\frac{2EI}{F}}\left[\sqrt{\cos(\alpha) - a_1} - \sqrt{\cos(\psi + \alpha) - a_1}\right] \tag{8}$$

with: $a_1 = cos(\psi_L + \alpha) - \frac{EI\left(k_{in} + \frac{M}{EI}\right)^2}{2F}$

Whereas, for the other coordinate, using the second of (4) and (6):

$$\xi(\psi) = \int_{\alpha_1}^{\psi+\alpha_1} \frac{\cos(\vartheta)}{\sqrt{\left(\frac{2F}{EI}\right)[cos(\vartheta) - cos(\psi_L + \alpha)] + \left(k_{in} + \frac{M}{EI}\right)^2}}\, d\vartheta \tag{9}$$

This integral focusses the nature of the problem, since it cannot be integrated using standard solutions. In [7] the author follows a procedure expressing a similar integral as: sum and difference of an incomplete elliptic integral of first kind, a complete elliptic integral of first kind, an incomplete elliptic integral of second kind and a complete elliptic integral of second kind, for both independent coordinates.

It is known in scientific literature, e.g. [26], that the complete and incomplete elliptic integrals of first and second kind are expressed as double series of functions (Kampé de Fériet or Appell series); therefore, this solution involves calculating four times a double hypergeometric function for each independent coordinates. This is the only fully analytical solution at our knowledge. As shown in the next steps, we will obtain a new closed-form solution (analytical) only using two times the hypergeometric function previously introduced; the computational advantage compared to the other analytic solution is straightforward.

With a simple substitution the starting point is:

$$\xi(\psi) = \sqrt{\frac{EI}{2F}} \int_{\alpha}^{\psi+\alpha} \frac{d\sin(\vartheta)}{\sqrt{\cos(\vartheta) - a_1}}$$

It is important to observe that $\cos(\vartheta) - a_1 > 0 \quad \forall\, \vartheta \in [\alpha, \psi + \alpha]\ ,\ \psi \in [0, \psi_L]$

Applying property (9):

$$\xi(\psi) = \sqrt{\frac{EI}{2F}} \int_{\alpha}^{\psi+\alpha} \sum_{n=0}^{\infty} \binom{-\frac{1}{2}}{n} [cos(\vartheta)]^{-\frac{1}{2}-n}\ (-a_1)^n\, dsin(\vartheta)$$

The series of functions is uniformly convergent (it is a series of powers evaluated in their radii of convergence) and it is possible to apply the series-integral exchange. Recurring to property (5) one gets:

$$\xi(\psi) = \sqrt{\frac{EI}{2F}} \sum_{n=0}^{\infty} \frac{\left(\frac{1}{2}\right)_n}{n!} (a_1)^n \int_{\alpha}^{\psi+\alpha} [1 - sin^2(\vartheta)]^{-\left(\frac{n}{2}+\frac{1}{4}\right)}\, d\, sin(\vartheta) \overset{\{9\}}{=}$$

$$= \sqrt{\frac{EI}{2F}} \sum_{n=0}^{\infty} \sum_{k=0}^{\infty} \frac{\left(\frac{1}{2}\right)_n}{n!} (a_1)^n\, \frac{\left(\frac{n}{2}+\frac{1}{4}\right)_k}{k!} \int_{\alpha}^{\psi+\alpha} [sin^2(\vartheta)]^k\, dsin(\vartheta) \overset{\{8\}}{=}$$

$$= \sqrt{\frac{EI}{2F}} \sum_{n=0}^{\infty} \sum_{k=0}^{\infty} \frac{\left(\frac{1}{2}\right)_n}{n!} (a_1)^n\, \frac{\left(\frac{n}{2}+\frac{1}{4}\right)_k \left(\frac{1}{2}\right)_k}{\left(\frac{3}{2}\right)_k}\, \frac{[sin(\vartheta)]^{2k+1}\Big|_{\alpha}^{\psi+\alpha}}{k!} \overset{\{1\}}{=}$$

$$= \sqrt{\frac{EI}{2F}} \sum_{n=0}^{\infty} \sum_{k=0}^{\infty} \frac{\left(\frac{1}{4}\right)_{\frac{n}{2}+k} \left(\frac{1}{2}\right)_n \left(\frac{1}{2}\right)_k}{\left(\frac{1}{4}\right)_{\frac{n}{2}} \left(\frac{3}{2}\right)_k}\, \frac{(a_1)^n\, [sin^{2k+1}(\psi+\alpha) - sin^{2k+1}(\alpha)]}{n!\ k!}$$

Taking advantage of the definition given to the previously introduced hypergeometric function:

$$\xi(\psi) = \sqrt{\frac{EI}{2F}} \left[sin(\psi+\alpha)\ {}_{0}^{\frac{1}{2}}\mathrm{I}\left(\begin{matrix} \frac{1}{4}, \frac{1}{2}, \frac{1}{2} \\ \frac{1}{4}, \frac{3}{2} \end{matrix} ; a_1, sin^2(\psi+\alpha) \right) - sin(\alpha)\ {}_{0}^{\frac{1}{2}}\mathrm{I}\left(\begin{matrix} \frac{1}{4}, \frac{1}{2}, \frac{1}{2} \\ \frac{1}{4}, \frac{3}{2} \end{matrix} ; a_1, sin^2(\alpha) \right) \right] \quad (10)$$

Whence the parametric equations of the beams result in the (*O*, *x*, *y*) reference, by basis change:

$$x(\psi) = \xi(\psi)cos(\alpha) + \eta(\psi)sin(\alpha)$$
$$y(\psi) = -\xi(\psi)sin(\alpha) + \eta(\psi)cos(\alpha) \qquad \psi \in [0, \psi_L]$$

It is crucial to highlight that another important hypothesis of the model is the monotonicity of the variable ψ in the deformed configuration.

The interval-end parameter ψ_L outcomes from the length conservation (the beam is inextensible).

This condition is guaranteed integrating eq. (6) and imposing the equality to *L* (beam length). The parameter ψ_L is also estimated applying the same hypergeometric series:

$$L = \sqrt{\frac{EI}{2F}} \int_{\alpha}^{\psi_L+\alpha} \frac{d\vartheta}{\sqrt{\cos(\vartheta) - a_1}} \overset{\{9\}}{=} \frac{1}{\sqrt{2A}} \int_{\alpha}^{\psi_L+\alpha} \sum_{n=0}^{\infty} \binom{-\frac{1}{2}}{n} (-a_1)^n \, [cos(\vartheta)]^{-\frac{1}{2}-n} d\vartheta \overset{\{5\}}{=}$$

$$= \sqrt{\frac{EI}{2F}} \sum_{n=0}^{\infty} \frac{\left(\frac{1}{2}\right)_n}{n!} (a_1)^n \int_{\alpha}^{\psi_L+\alpha} [1 - sin^2(\vartheta)]^{-\left(\frac{3}{4}+n\right)} \, dsin(\vartheta) \overset{\{9,5\}}{=}$$

$$= \sqrt{\frac{EI}{2F}} \sum_{n=0}^{\infty} \sum_{k=0}^{\infty} \frac{\left(\frac{1}{2}\right)_n}{n!} (a_1)^n \, \frac{\left(\frac{n}{2}+\frac{3}{4}\right)_k}{k!} \int_{\alpha}^{\psi_L+\alpha} [sin(\vartheta)]^{2k} \, dsin(\vartheta) \overset{\{1\}}{=}$$

$$= \sqrt{\frac{EI}{2F}} \sum_{n=0}^{\infty} \sum_{k=0}^{\infty} \frac{\left(\frac{3}{4}\right)_{\frac{n}{2}+k} \left(\frac{1}{2}\right)_n \left(\frac{1}{2}\right)_k}{\left(\frac{3}{4}\right)_{\frac{n}{2}} \left(\frac{3}{2}\right)_k} \, \frac{(a_1)^n \, [sin^{2k+1}(\psi_L + \alpha) - sin^{2k+1}(\alpha)]}{n! \; k!}$$

Whence, it results:

$$L = \sqrt{\frac{EI}{2F}} \left[sin(\psi_L + \alpha) \; {}_2^{\frac{1}{2}}\mathrm{I}_0 \left(\begin{matrix} \frac{3}{4}, \frac{1}{2}, \frac{1}{2} \\ \frac{3}{4}, \frac{3}{2} \end{matrix} ; \, a_1, sin^2(\psi_L + \alpha) \right) - sin(\alpha) \; {}_2^{\frac{1}{2}}\mathrm{I}_0 \left(\begin{matrix} \frac{3}{4}, \frac{1}{2}, \frac{1}{2} \\ \frac{3}{4}, \frac{3}{2} \end{matrix} ; \, a_1, sin^2(\alpha) \right) \right] \quad (11)$$

For the specific case $F_y = 0$, $F_x \neq 0$ (typical buckling load) the angle $\alpha = 0$, the previous equation is restricted to only the first hypergeometric function.

3.3 Solution for F_x positive configuration

The solution of F_x positive case - Fig.1.(b) develops similarly to the previous one (in this case F_x considered negative in eq. (1)). For this reason, the full analytical steps are not reported. This configuration holds when $\frac{\pi}{2} \leq \alpha < \pi$.

For convenience, the substitution $\alpha^* = \alpha - \frac{\pi}{2}$ is introduced. The curvature- angle ϑ relationship is:

$$ds = \frac{d\vartheta}{\sqrt{\left(\frac{2F}{EI}\right)[sin(\vartheta_L) - sin(\vartheta)] + \left(k_{in} + \frac{M}{EI}\right)^2}} \tag{12}$$

Where $\vartheta(s) = \psi(s) + \alpha^*$

Use second of eq.s (4) and (12) one obtains:

$$\xi(\psi) = \int_{\alpha^*}^{\psi+\alpha^*} \frac{cos(\vartheta)}{\sqrt{\left(\frac{2F}{EI}\right)[sin(\psi_L + \alpha^*) - sin(\vartheta)] + \left(k_{in} + \frac{M}{EI}\right)^2}} d\vartheta$$

This last is, similarly to (7), an Abelian's integral; solving it and enforcing the substitution $\alpha^* = \alpha - \frac{\pi}{2}$:

$$\xi(\psi) = \sqrt{\frac{2EI}{F}}\left[\sqrt{\cos(\alpha) + a_2} - \sqrt{\cos(\psi + \alpha) + a_2}\right] \tag{13}$$

with: $a_2 = \frac{EI\left(k_{in} + \frac{M}{EI}\right)^2}{2F} - cos\left(\psi_L + \alpha\right)$.

Using instead last of eq.s (4) and (9):

$$\eta(\psi) = \int_{\alpha^*}^{\psi+\alpha^*} \frac{sin(\vartheta)}{\sqrt{\left(\frac{2F}{EI}\right)[sin(\psi_L + \alpha_2) - sin(\vartheta)] + \left(k_{in} + \frac{M}{EI}\right)^2}} d\vartheta$$

This last integral is approached with hypergeometric function as already done for eq. (9). Similar steps as before are not detailed, but more attention is given for the calculations concerning the parameter β.

It is possible to write the previous one as:

$$\eta(\psi) = \sqrt{\frac{EI}{2F}} \int_{\psi+\alpha^*}^{\alpha^*} \frac{d\cos(\vartheta)}{\sqrt{a_2 - \sin(\vartheta)}}$$

$a_2 - \sin(\vartheta) > 0 \quad \forall\, \vartheta \in [\alpha^*, \psi + \alpha^*]\ ,\ \psi \in [0, \psi_L]$

Applying chronologically, as done previously, properties {9}, {5}, {9}, and {8} one obtains:

$$\eta(\psi) = \sqrt{\frac{EI}{2F}} \sum_{n=0}^{\infty} \sum_{k=0}^{\infty} \frac{\left(\frac{1}{2}\right)_n}{n!} (a_2)^{-\frac{1}{2}-n} \frac{\left(-\frac{n}{2}\right)_k \left(\frac{1}{2}\right)_k}{\left(\frac{3}{2}\right)_k} \frac{[cos(\vartheta)]^{2k+1}\Big|_{\psi+\alpha^*}^{\alpha^*}}{k!}$$

Observing that:

$$\left(-\frac{n}{2}\right)_k = \left(\beta - \left(\beta + \frac{n}{2}\right)\right)_k \overset{\{1\}}{=} \frac{(\beta)_{-\beta-\frac{n}{2}+k}}{(\beta)_{-\beta-\frac{n}{2}}} \qquad \forall\, \beta \in \mathbb{R}\backslash\{\mathbb{Z}^-, 0\},\ n \neq 2j\ \wedge\ j \geq 0$$

One finds the solution in terms of hypergeometric function

$$\eta(\psi) = \sqrt{\frac{EI}{2F}} \frac{1}{\sqrt{a_2}} \sum_{n=0}^{\infty} \sum_{k=0}^{\infty} \frac{(\beta)_{-\beta-\frac{n}{2}+k} \left(\frac{1}{2}\right)_n \left(\frac{1}{2}\right)_k}{(\beta)_{-\beta-\frac{n}{2}} \left(\frac{3}{2}\right)_k} \frac{\left(\frac{1}{a_2}\right)^n [cos^{2k+1}(\alpha^*) - cos^{2k+1}(\psi+\alpha^*)]}{n!\ k!}$$

Replacing $\alpha^* = \alpha - \frac{\pi}{2}$:

$$\eta(\psi) = \sqrt{\frac{EI}{2F}} \frac{1}{\sqrt{a_2}} \left[\sin(\alpha)\ {}^{-\frac{1}{2}}_{-\beta}\mathrm{I}\left(\begin{matrix}\beta, \frac{1}{2}, \frac{1}{2} \\ \\ \beta, \frac{3}{2}\end{matrix}; \frac{1}{a_2}, sin^2(\alpha)\right) - sin(\psi+\alpha)\ {}^{-\frac{1}{2}}_{-\beta}\mathrm{I}\left(\begin{matrix}\beta, \frac{1}{2}, \frac{1}{2} \\ \\ \beta, \frac{3}{2}\end{matrix}; \frac{1}{a_2}, sin^2(\psi+\alpha)\right) \right]$$

$$\forall\, \beta \in \mathbb{R}\backslash\{\mathbb{Z}^-, 0\},\ n \neq 2j\ \wedge\ j \geq 0 \qquad (14)$$

Just above conditions are necessary in order that the rising factorial, then the Gamma function, is defined.

The parametric equations of the beams for this case are written in (O, *x*, *y*) reference through a basis change:

$$\begin{aligned} x(\psi) &= \xi(\psi)sin(\alpha) - \eta(\psi)cos(\alpha) \\ y(\psi) &= \xi(\psi)cos(\alpha) + \eta(\psi)sin(\alpha) \end{aligned} \qquad \psi \in [0, \psi_L] \qquad (15)$$

Again, the parameter ψ_L is obtained through the length conservations in (12). Similarly as before:

$$L = \sqrt{\frac{EI}{2F}} \frac{1}{\sqrt{a_2}} \left[\sin(\alpha)\ {}^{-\frac{1}{2}}_{0}\mathrm{I}\left(\begin{matrix}\frac{1}{2}, \frac{1}{2}, \frac{1}{2} \\ \\ \frac{1}{2}, \frac{3}{2}\end{matrix}; \frac{1}{a_2}, sin^2(\alpha)\right) - sin(\psi_L+\alpha)\ {}^{-\frac{1}{2}}_{0}\mathrm{I}\left(\begin{matrix}\frac{1}{2}, \frac{1}{2}, \frac{1}{2} \\ \\ \frac{1}{2}, \frac{3}{2}\end{matrix}; \frac{1}{a_2}, sin^2(\psi_L+\alpha)\right) \right]$$

$$n \neq 2j+1\ \wedge\ j \geq k \qquad (16)$$

The above limitation arises for Gamma function consistency.

It is useful to observe that the deformed configuration of a cantilever beam loaded at the end with a simply vertical load is obtained by this solution (F_x positive), posing $F_x = 0$.

4. Strategy to compute the Hypergeometric series and tolerance criterion

The hypergeometric series owe their wide diffusion to the simplicity wherewith they are calculated. Their strength is to express the coefficients of the series in a recursive form, demanding a low computational cost. One of most general definitions of hypergeometric series is due to J. Horn (1889) [27]. "The double power series"

$$\sum_{n=0}^{\infty}\sum_{k=0}^{\infty} A_{nk}\ x^n y^k$$

is a hypergeometric series if the two quotients

$$\frac{A_{n+1,k}}{A_{n,k}} = f(n,k) \quad and \quad \frac{A_{n,k+1}}{A_{n,k}} = g(n,k)$$

are rational functions of n and k."

Expressing, for convenience, $(a)_{\beta+\gamma n+k} \overset{\{7\}}{=} (a)_{\beta+\gamma n}\,(a+\beta+\gamma n)_k$ the new hypergeometric series looks like:

$${}^{\gamma}_{\beta}\mathrm{I}\left(\begin{matrix} a\ ,\ b_1\ ,b_2 \\ c_1\ ,c_2 \end{matrix}\ ;\ x,y\right) = \sum_{n=0}^{\infty}\sum_{k=0}^{\infty} \frac{(a)_{\beta+\gamma n}(a+\beta+\gamma n)_k\,(b_1)_n\,(b_2)_k}{(c_1)_{\beta+\gamma n}\,(c_2)_k}\,\frac{x^n\,y^k}{n!\,k!}$$

Apply the previous definitions, using the properties 1) and the recursive formula for Gamma function $\Gamma(x)=(x-1)\,\Gamma(x-1)$, it is easy to get:

$$\frac{A_{n+1,k}}{A_{n,k}} = \frac{(a+\beta+\gamma n+k)_\gamma (b_1+n)}{(c_1+\beta+\gamma n)_\gamma}\,\frac{1}{n+1} \quad ; \quad \frac{A_{n,k+1}}{A_{n,k}} = \frac{(a+\beta+\gamma n+k)(b_2+k)}{(c_2+k)}\,\frac{1}{k+1}$$

These recurrence relations are fundamental for the speed computation of the hypergeometric function. The calculation of series terms is therefore easily automatable as:

$$B_{0,n} = 1 \quad ; \quad {}^1S_{0,n} = B_{0,n}$$

$$B_{k+1,n} = B_{k,n}\,\frac{(a+\beta+\gamma n+k)(b_2+k)}{(c_2+k)}\,\frac{y}{k+1} \quad ; \quad {}^1S_{k+1,n} = {}^1S_{k,n} + B_{k+1}$$

Now, an arrest criterion (or tolerance criterion) is needed. A trivial, but effective criterion is stopping the *k*-summation when:

$$\frac{|B_{K+1,n}|}{|{}^1S_{K,n}|} < tol \quad ; \quad \frac{|B_{K,n}|}{|{}^1S_{K-1,n}|} < tol$$

Where *tol* is a tolerance to neglect the $K+1_{th}$ terms of *k*-summation by respect to the total sum of terms until the K_{th} term. Being *K* the number of terms that satisfy the tolerance, ${}^1S_{K,n}$ is the sum of *k*-summation at the fixed *n* index; then the *n*-summation starts:

$$C_0 = {}^1S_{K,0} \quad ; \quad {}^2S_0 = C_0$$

$$C_{n+1} = C_n \frac{(a+\beta+\gamma n+k)_\gamma (b_1+n)}{(c_1+\beta+\gamma n)_\gamma} \frac{x}{n+1} {}^1S_{K,n} \; ; \quad {}^2S_{n+1} = {}^2S_n + C_{n+1}$$

Similar as done above for *k*, the tolerance criterion to stop *n*-summations is:

$$\frac{|C_{N+1}|}{|{}^2S_N|} < tol \quad ; \quad \frac{|C_N|}{|{}^2S_{N-1}|} < tol$$

${}^2S_N$ is the total sum of hypergeometric series ${}^{\gamma}_{\beta}\mathrm{I}\left(\begin{matrix} a\,,\ b_1\ ,b_2 \\ c_1\,,c_2 \end{matrix}; x, y\right)$.

5. Applications, Extensions to other configurations and numerical examples

In this section, various examples concerning the applications of the proposed mathematical model are shown. We start with the simplest case of a cantilever beam, supported by hinged-roller and various end-displacements and end-angle curves for F_x negative and F_x positive cases. Then, the cases of follower end-load configurations are studied. The mathematical model is furtherly extended to spring-hinged (compliant clamped) cantilever beams and finally, the case of clamped beams loaded trough a fixed point is discussed. The workflow of the conservative load cases is represented in Fig.2

It is important to highlight that the eq.s (11,16) from which the ψ_L angle is derived are implicit equations; therefore, the unknown angle should be iteratively computed. This hurdle is not a consequence of the hypergeometric function approach, but it also occurs when dealing with elliptic integrals; again it is necessary to follow an iterative search for the angle ψ_L. The reason is that the differential equation (1 or 3) is strongly non-linear and nothing better can be done. Therefore, the most expensive computation effort

regards the angle ψ_L. At every tentative solution, the integrals of eq.s (6 or 12) must be solved, so that the computational advantage repeats at every iteration step. Paragraph 6 is intended to clarify this point.

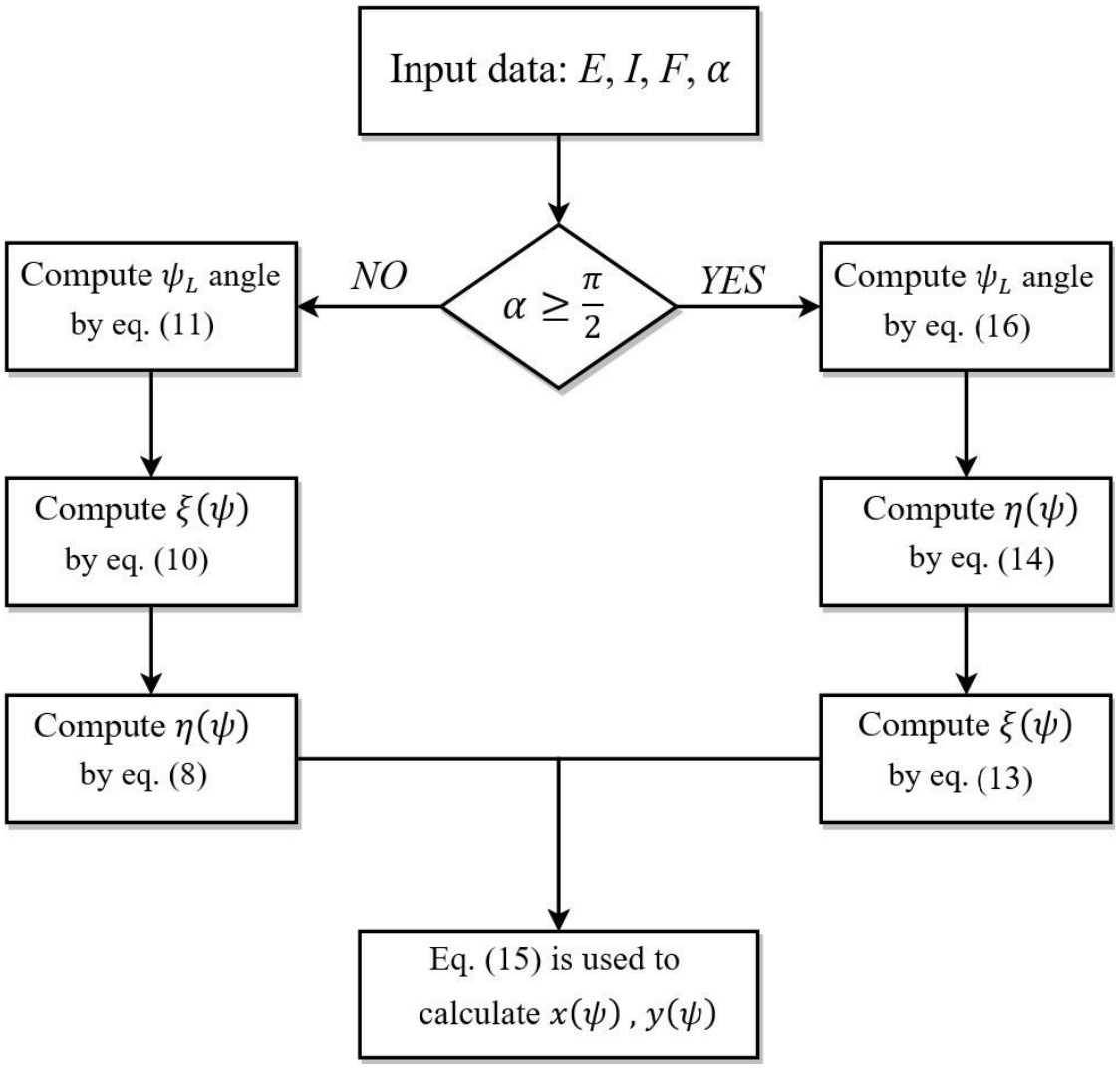

Fig. 2. Computing steps workflow for conservative load case

5.1 Cantilever beam

The first application regards a straight cantilever beam, loaded by two forces, separately applied, with same modulus but different angles of inclination. The resulting two configurations are the F_x negative and F_x positive ones. The value of thick and wide of rectangular section, the length of the beam and the Young's modulus are reported in Fig.3, together with the numerical results given for comparison.

The analytical results are compared with the finite element method.

The end-displacement values and angles are, respectively, $x_L = 707.2$ mm, $y_L = 633.6$ mm and $\psi_L = 61.86°$ for F_x negative and $x_L = 901.0$ mm, $y_L = 396.9$ mm and $\psi_L = 34.55°$ for F_x positive.

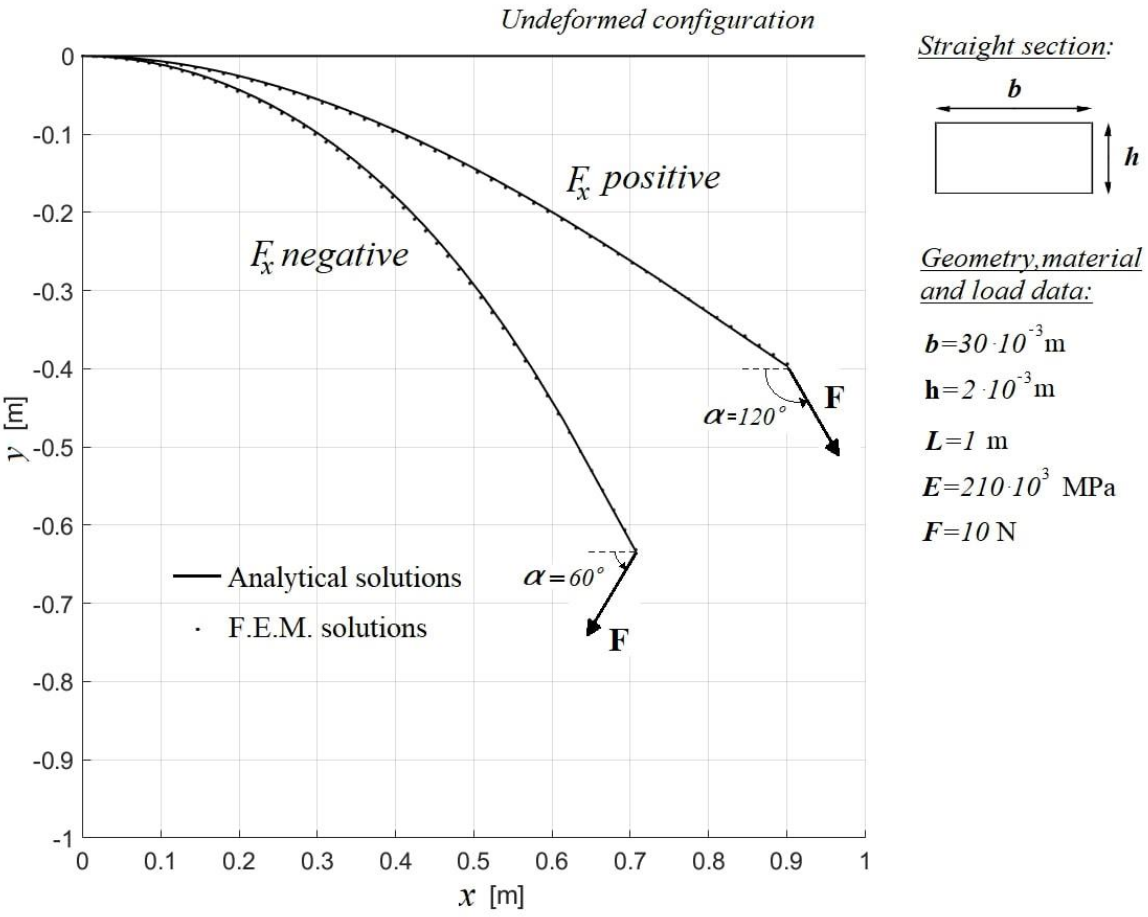

Fig. 3. Displacement of a straight cantilever beam in F_x negative and F_x positive configurations

5.2 Hinged-roller support curved beam – Buckling case

Consider the initially constant curvature (arc) beam with hinged and roller support constraints, subjected to a load collinear to *x*-axis in Fig.4 (the dashed line is the initial beam). This is a classic example of buckling configuration. Apparently, this case would require a new solution of the differential equilibrium equation, but if one observes that at the middle point $\psi = 0$ (symmetry holds) and that at the ends the hinges do not constrain the rotations, the deformed configuration can be seen as two cantilever beams $\frac{L}{2}$ long, locked at the middle point and loaded at the other end. So, the F_x negative configuration represents this case.

The buckling curves are given according to ratio $\frac{F}{F_{cr}}$ where $F_{cr} = \left(\frac{\pi}{2\,\mathrm{L}}\right)^2 EI$ is the Euler critical load of an equivalent straight beam. The section geometry and material data are the same of example 5.1, but an

initial curvature of $k_{in} = 1\ \mathrm{m}^{-1}$ is assumed. It is clear that, in this case, the angle $\alpha = 0$.

For this example, it is particularly convenient to check the convergence speed of hypergeometric series. In fact, since the angle $\alpha = 0$, then the F_x negative solution is represented by a single term of the hypergeometric series. To this goal, we provide in Table indicating the number of terms *n* and *k* used for computing the end-displacement *x* and end-angle ψ_L (*y* end-displacement is calculated without hypergeometric series, by analytic formula*)* as a function of $\frac{F}{F_{cr}}$ ratio.

From the previous tables it appears that the computational cost, that is the numbers of terms required for the prescribed tolerance which is chosen equal to 10^{-4}, increases with the ratio $\frac{F}{F_{cr}}$, namely if the end-load increases. The dimensionless variables that appear in all expressions give the advantage that the prescribed tolerance is independent of the specific geometry or loads.

It is evident that the endpoint has been chosen for this discussion because this is also the point requiring the largest number of terms for convergence.

5.3 Technical design curves of end-point displacements for F_x negative and F_x positive cases

It is important to highlight that these analytic solutions present the advantage to calculate the displacement even of a single point, avoiding the integration throughout the full length of the beam, unlike what is required by the numerical methods listed in the introduction. In many applications, the highest interest is to know the displacements of the final point, which is the point with the greatest displacements.

At a first glance, the presented solutions appear a little bit tough, and they mandatory require a numerical computing environment. For these reasons, we create dimensionless curves, from which it is easy and quick to evaluate the end displacements.

The graphs obtained concerns beams initially straight; they make use of equations 8),10),11) for F_x negative case - Fig.5.(a.b.c) and 13),14),15) for F_x positive case - Fig.6.(a.b.c), in a dimensionless axis representation

$\sqrt{\frac{F}{EI}}\,\eta(\psi)$, $\sqrt{\frac{F}{EI}}\,\xi(\psi)$. The angle α, concerning load orientation, is set as a parameter.

A simple explanation of how to use these graphs is provided, using a beam with the same data given in Fig.3 but twice long, namely *2 m*. With this data we get the adimensional abscissa of Fig.5.(a) $\sqrt{\frac{F}{EI}}L \approx 3.08$, giving a n angle value $\psi_L \approx 108°$. With this value, we get $\sqrt{\frac{F}{EI}}x_L \approx 0.45$ from Fig.5.(b) and $\sqrt{\frac{F}{EI}}y_L \approx 2.65$ from Fig.5.(c). Thus, the end-point displacement is $x_L \approx 0.29$ m and $y_L \approx 1.72$ m.

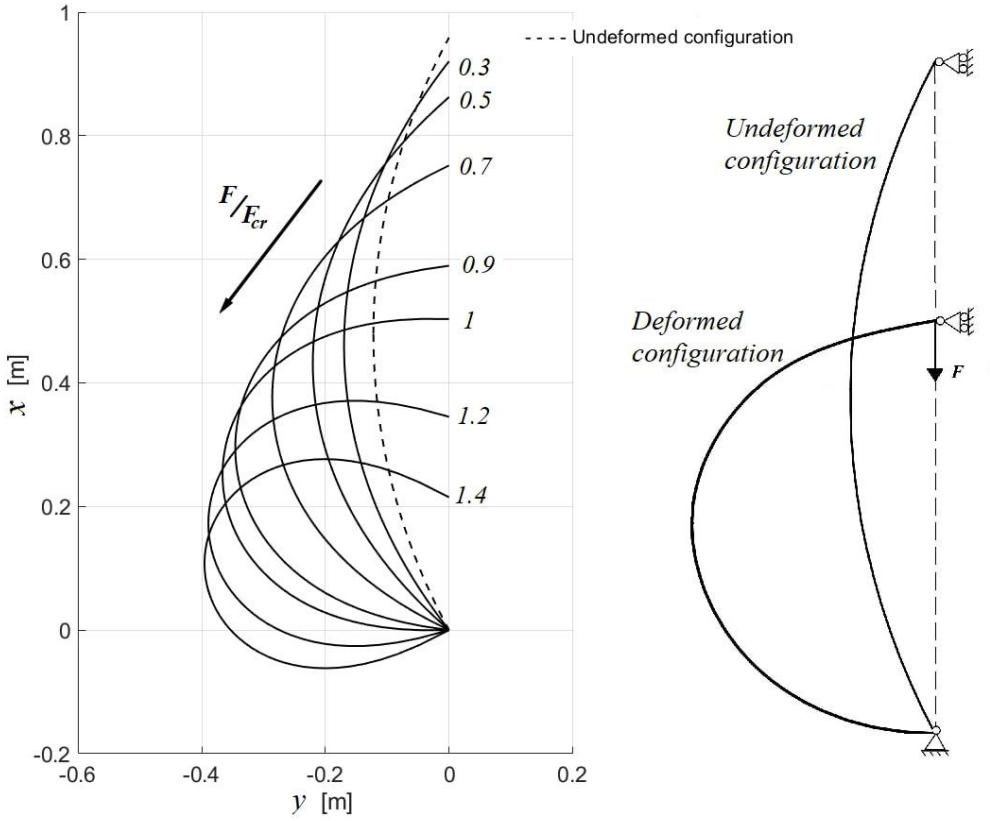

Fig. 4. Displacements of the arc beam hinged-roller supported in Buckling configurations

Table 1 Numbers of terms of hypergeometric function used to compute *x* end-displacement and ψ_L angle for ratio $\frac{F}{F_{cr}} = \{0.5\ ,1\ ,1.4\ \}$ and *tol*=10^{-4}

F/Fcr=0.5				F/Fcr=1				F/Fcr=1.4			
x end	displacement	ψ_L	angle	x end	displacement	ψ_L	angle	x end	displacement	ψ_L	angle
n	k	n	k	n	k	n	k	n	k	n	k
0	4	0	5	0	4	0	5	0	4	0	6
1	5	1	5	1	5	1	6	1	6	1	7
2	5	2	6	2	6	2	6	2	7	2	7
3	6	3	6	3	6	3	7	3	7	3	8
4	6	4	7	4	7	4	8	4	8	4	9
5	7	5	7	5	8	5	8	5	9	5	9
6	7	6	8	6	8	6	9	6	9	6	10
n_{tot}	6	n_{tot}	6	7	9	7	9	7	10	7	11
k_{tot}	40	k_{tot}	44	8	9	8	10	8	11	8	11
				9	10	9	10	9	11	9	12
				10	10	10	11	10	12	10	13
				n_{tot}	10	n_{tot}	10	11	13	11	13
				k_{tot}	82	k_{tot}	89	12	13	12	14
								13	14	13	14
								n_{tot}	13	n_{tot}	13
								k_{tot}	134	k_{tot}	144

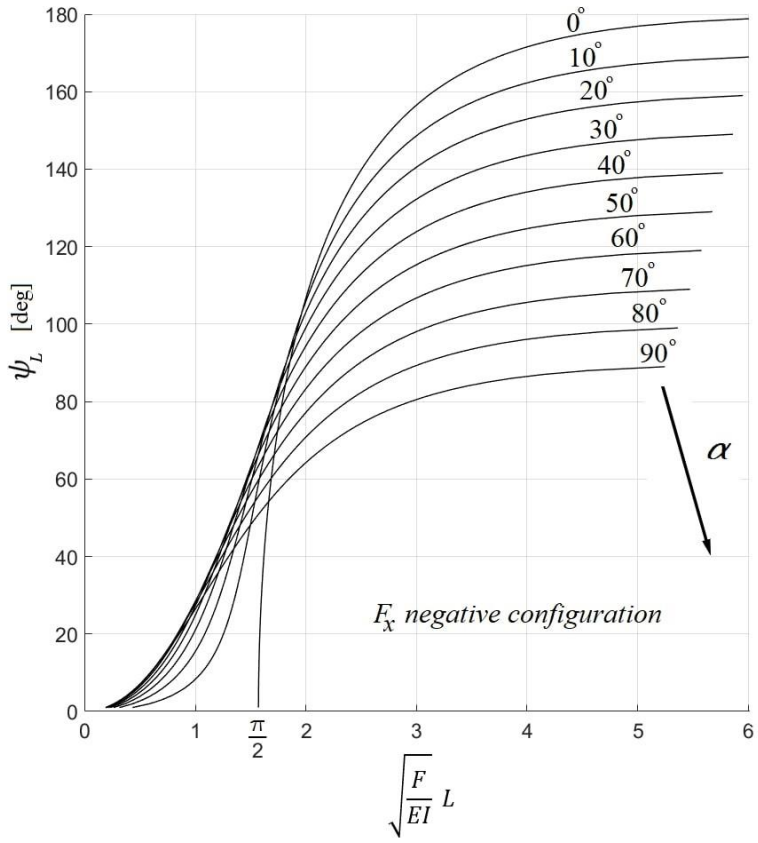

Fig. 5. (a) F_x negative configuration: ψ_L angle as function of dimensionless term $\sqrt{\frac{F}{EI}}L$ and parameter α

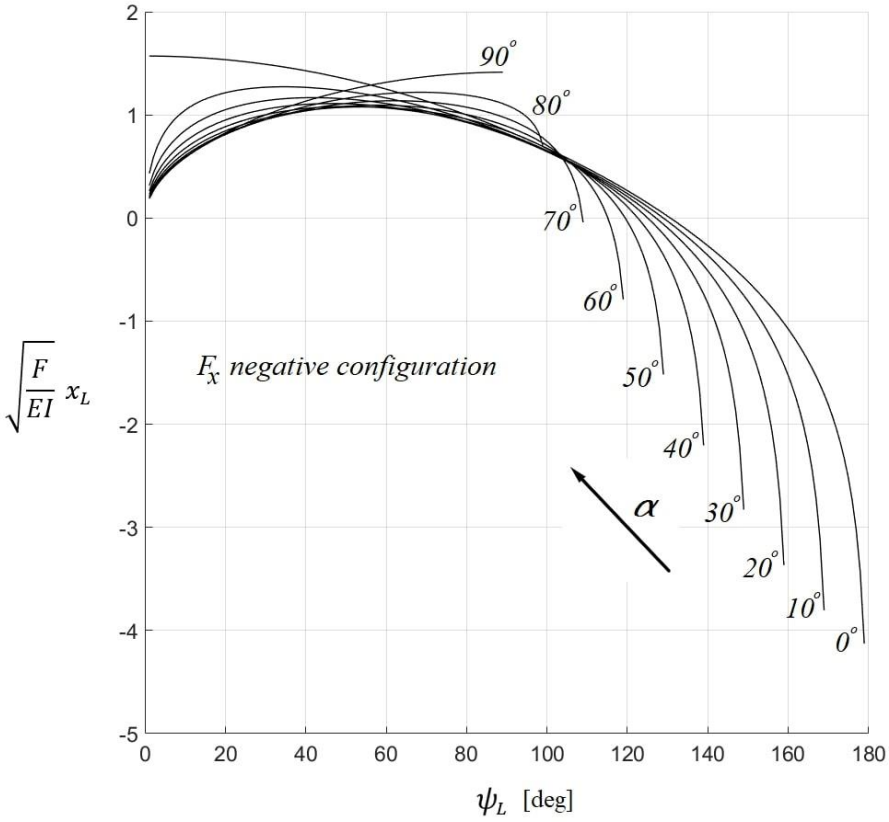

Fig. 5. (b) F_x negative configuration: dimensionless term $\sqrt{\frac{F}{EI}}x_L$ as function of ψ_L angle and parameter α

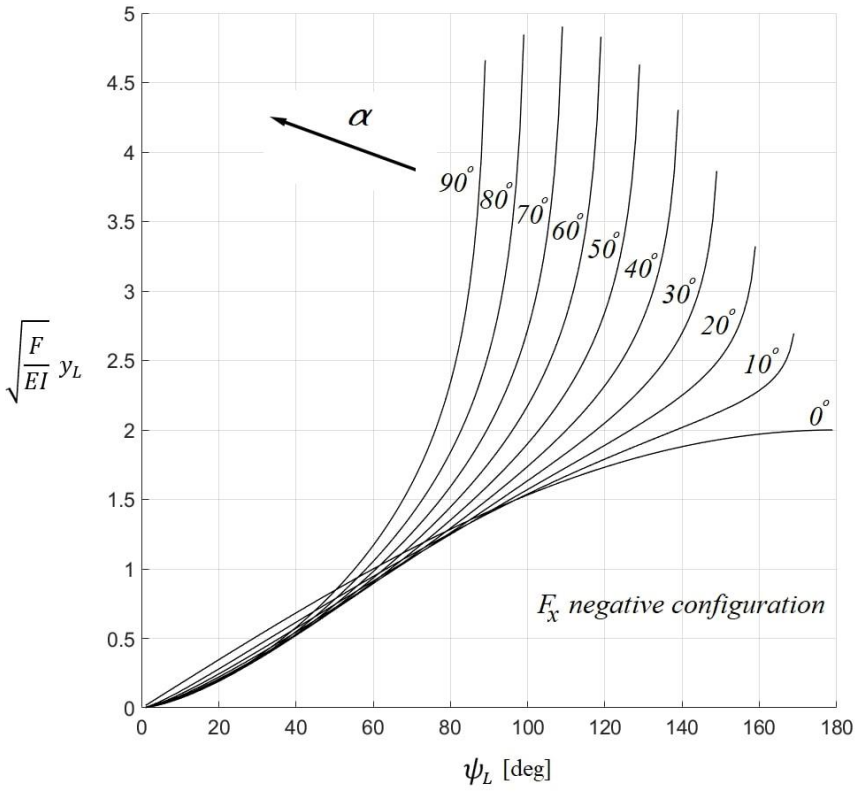

Fig. 5. (c) F_x negative configuration: dimensionless term $\sqrt{\frac{F}{EI}}y_L$ as function of ψ_L angle and parameter

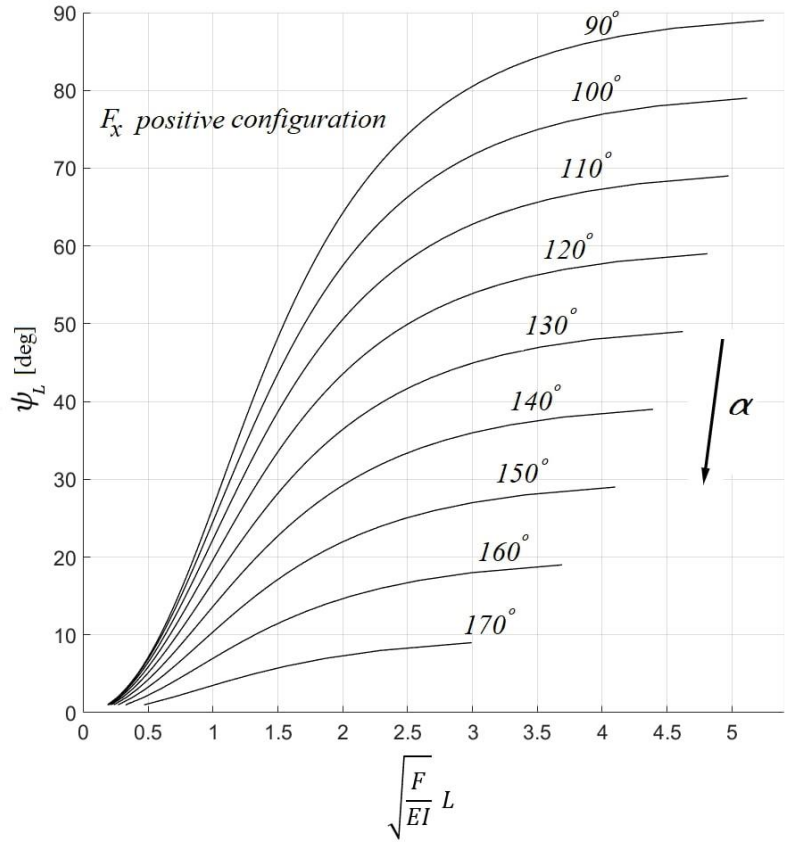

Fig.6. (a) F_x positive configuration: ψ_L angle as function of dimensionless term $\sqrt{\frac{F}{EI}}L$ and parameter α

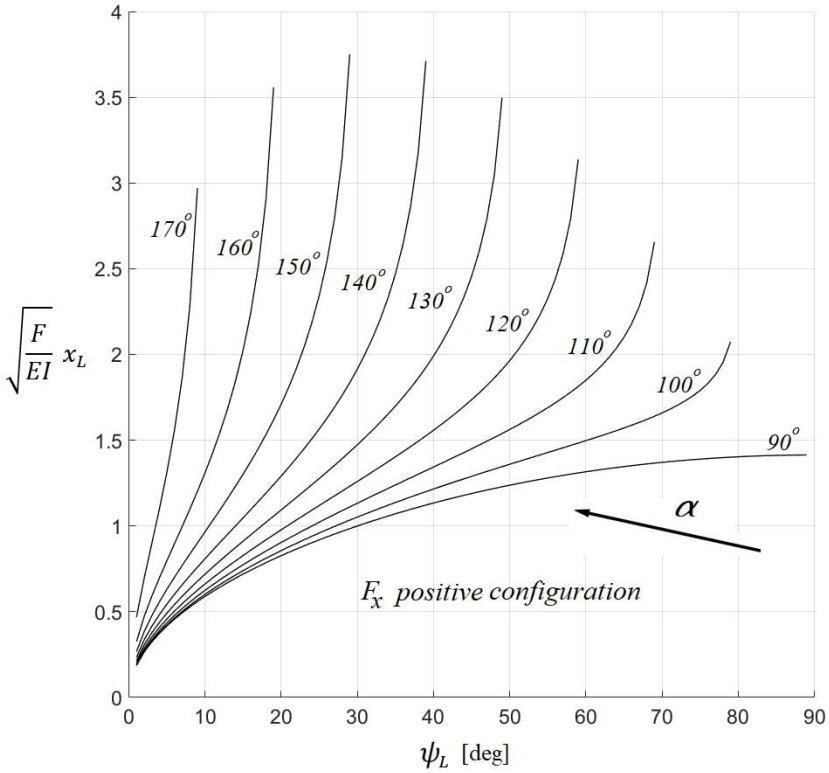

Fig. 6. (b) F_x positive configuration: dimensionless term $\sqrt{\frac{F}{EI}}x_L$ as function of ψ_L angle and parameter α

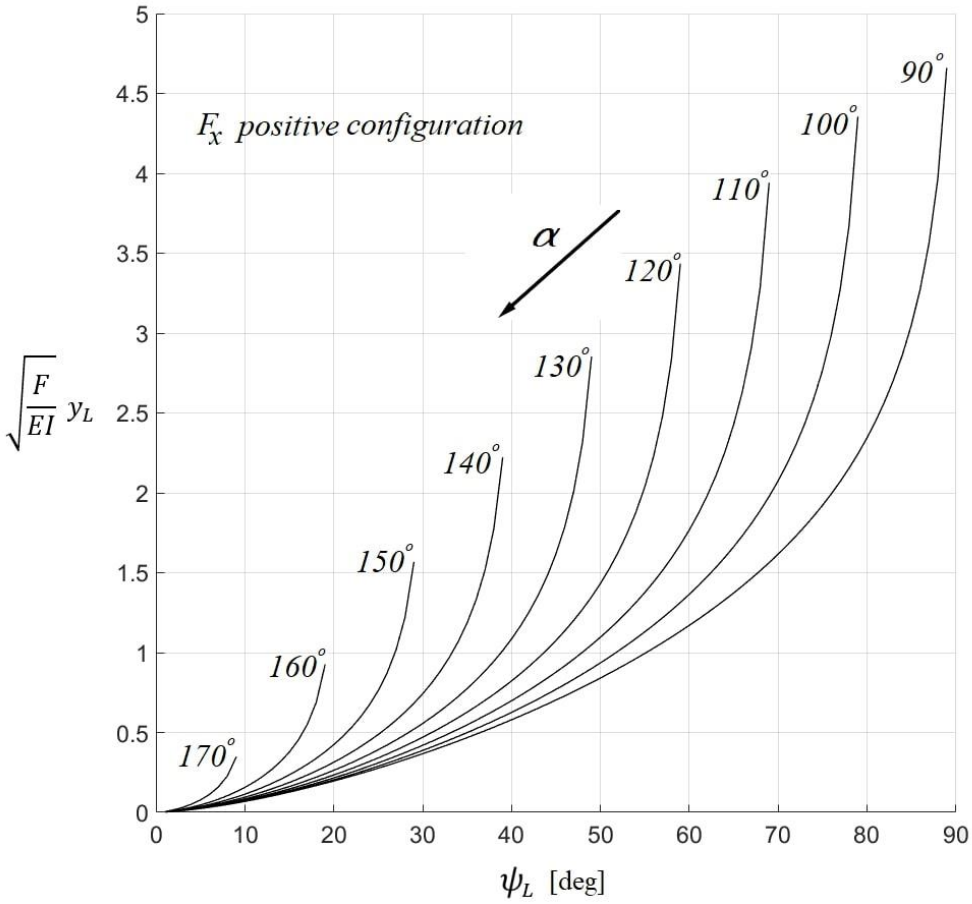

Fig.6. (c) F_x positive configuration: dimensionless term $\sqrt{\frac{F}{EI}}y_L$ as function of ψ_L angle and parameter α

5.4 Cantilever beam subject to end- follower load

A special type of loading, technically interesting, is the *follower load* [15,28]. This type of load has the particular property to keep the same angle of inclination of the load by respect to the end-tangent line. A more effective way to understand this type of load is to imagine that in every intermediate configuration the load rearranges in such a way to maintain the prescribed angle by respect to the normal/tangent unit vector. Again, the problem is divided into a *positive or negative configuration* of F_x .

In this case, the definitions F_x negative and F_x positive configurations requires additional information. In fact, the F_x positive case can project in the negative direction in the deformed configuration and vice-versa. Therefore, in this application we define as *initially F_x negative* the configuration that has, in the unloaded state, F_x negative (namely directed opposite to *x* axis), and *initially F_x positive* if in the undeformed state F_x is positive. In Fig.7, dashed lines in the undeformed state represent these virtual loads. Being φ the angle between the force direction and the tangent vector of the end-point, counter clockwise, the two different configurations depend on the value of this last angle:

$0 \leq \varphi < \frac{\pi}{2}$ the configuration is initially *F_x negative*

$\frac{\pi}{2} \leq \varphi < \pi$ the configuration is initially *F_x positive*

Taking advantage of this discrimination, the previous solutions are still valid, if the angle α is considered as $\alpha = \varphi - \psi_L$.

An example of numerical calculation is therefore proposed in both analysed cases in Fig.8; the geometric and material data of the beam is the same of Fig.3.

The Fig.9.(a.b.c) represent the technical design curves (initially F_x *negative*) for the end-point displacements and angle, similarly as done in § 5.3., now using the angle φ as a parameter.

Fig. 10.(a.b.c) regard the initially F_x *positive*.

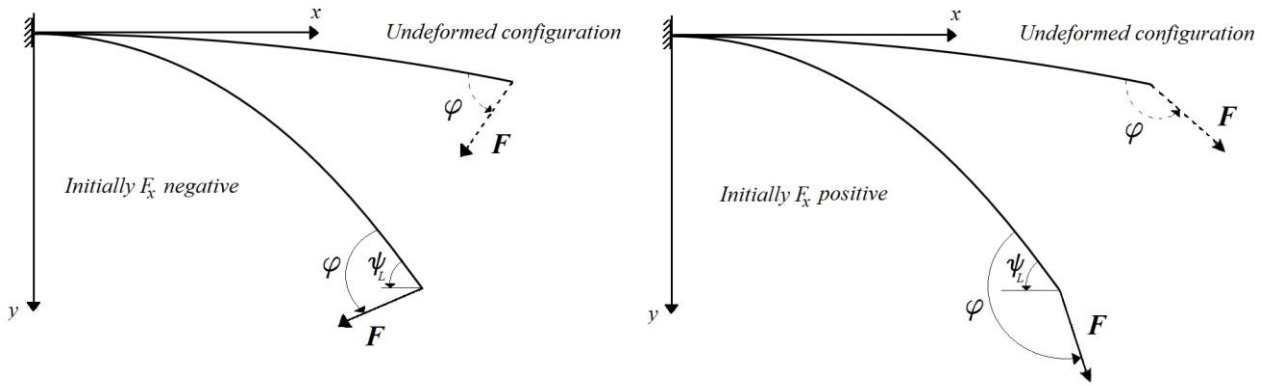

Fig.7. Cantilever beam with follower load in initially F_x negative and positive configurations.

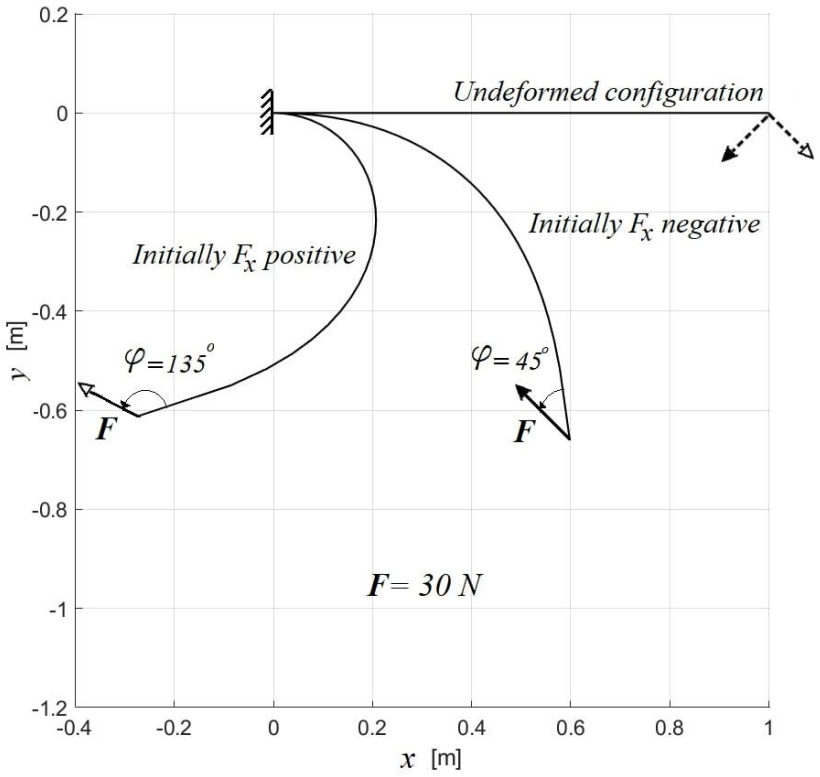

Fig.8. Cantilever beam subjected to initially F_x negative and initially F_x positive follower loads

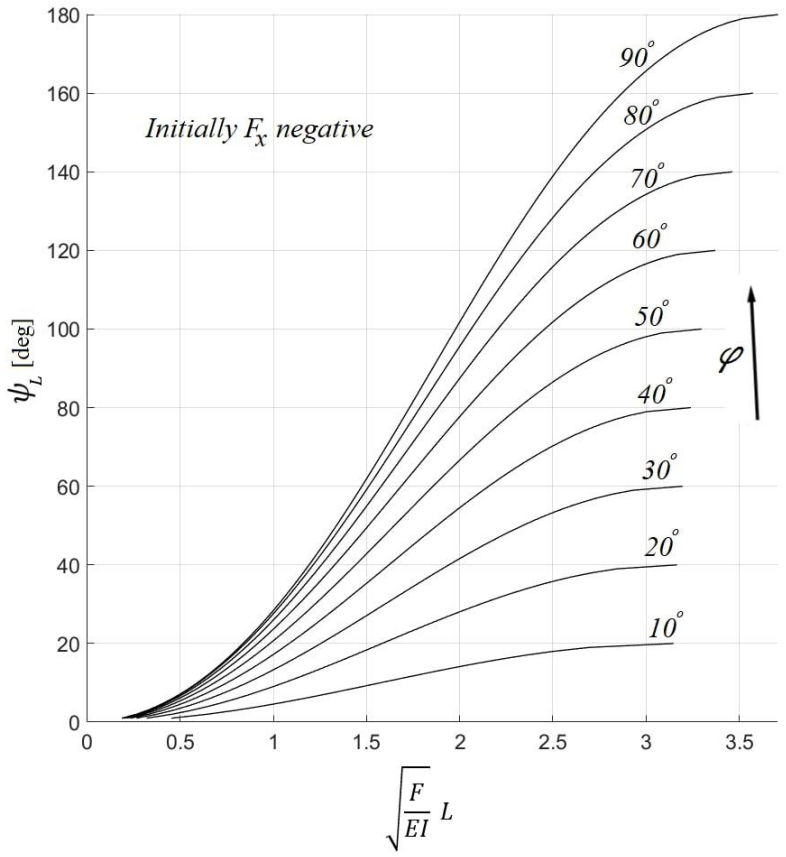

Fig.9. (a) Initially F_x negative follower load: ψ_L angle as function of dimensionless term $\sqrt{\frac{F}{EI}}L$ and parameter φ

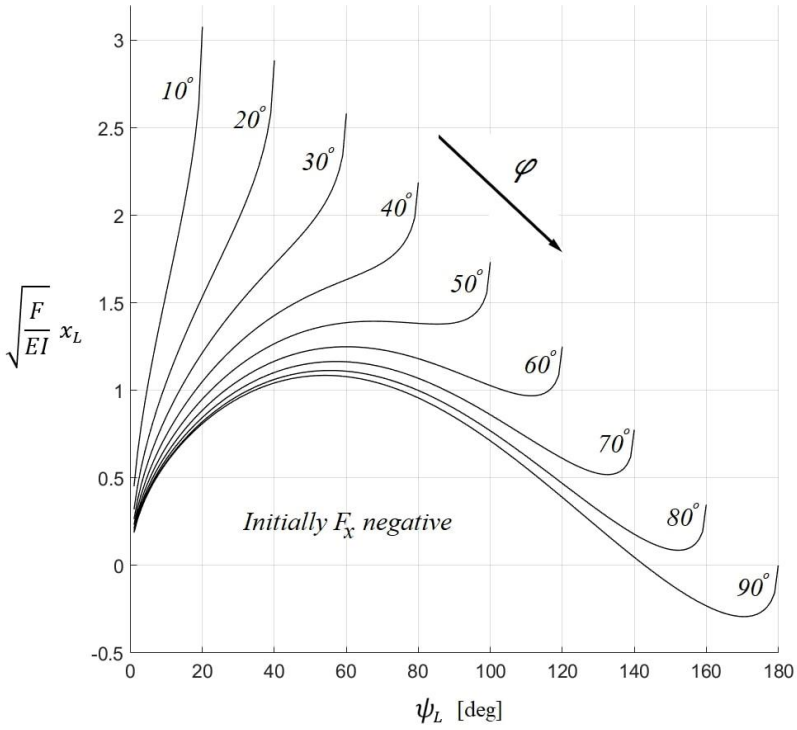

Fig. 9. (b) Initially F_x negative follower load: dimensionless term $\sqrt{\frac{F}{EI}}x_L$ as function of ψ_L angle and parameter φ

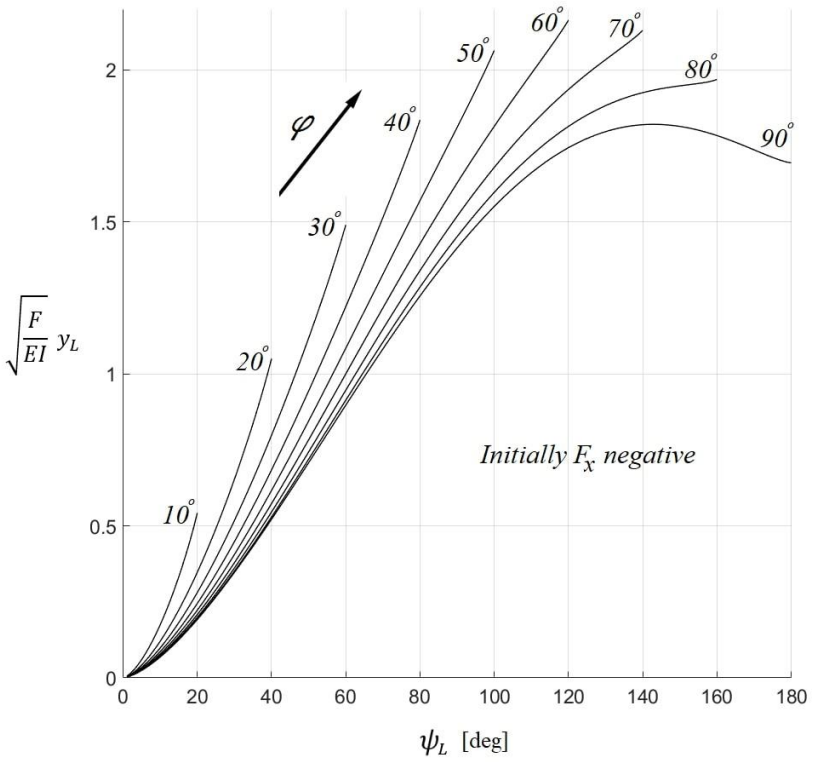

Fig.9. (c) Initially F_x negative follower load: dimensionless term $\sqrt{\frac{F}{EI}}y_L$ as function of ψ_L angle and parameter φ

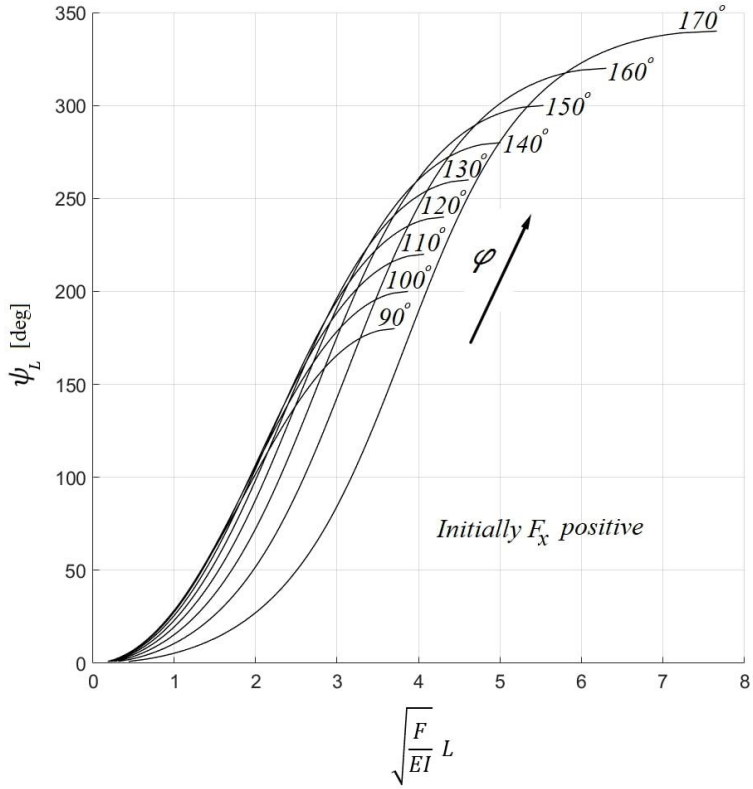

Fig.10. (a) Initially F_x positive follower load: ψ_L angle as function of dimensionless term $\sqrt{\frac{F}{EI}}L$ and parameter φ

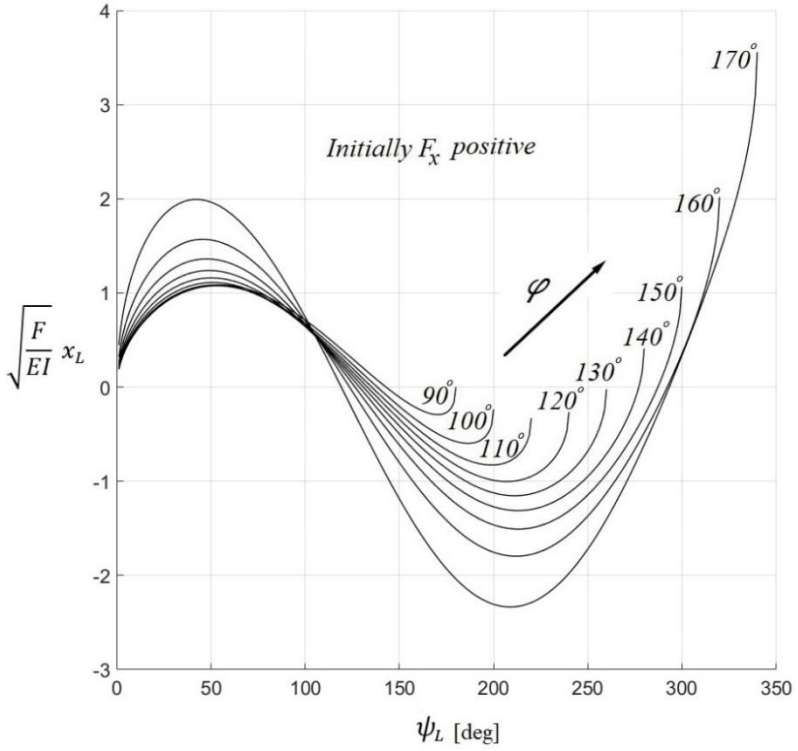

Fig. 10 (b) Initially F_x positive follower load: dimensionless term $\sqrt{\frac{F}{EI}}x_L$ as function of ψ_L angle and parameter φ

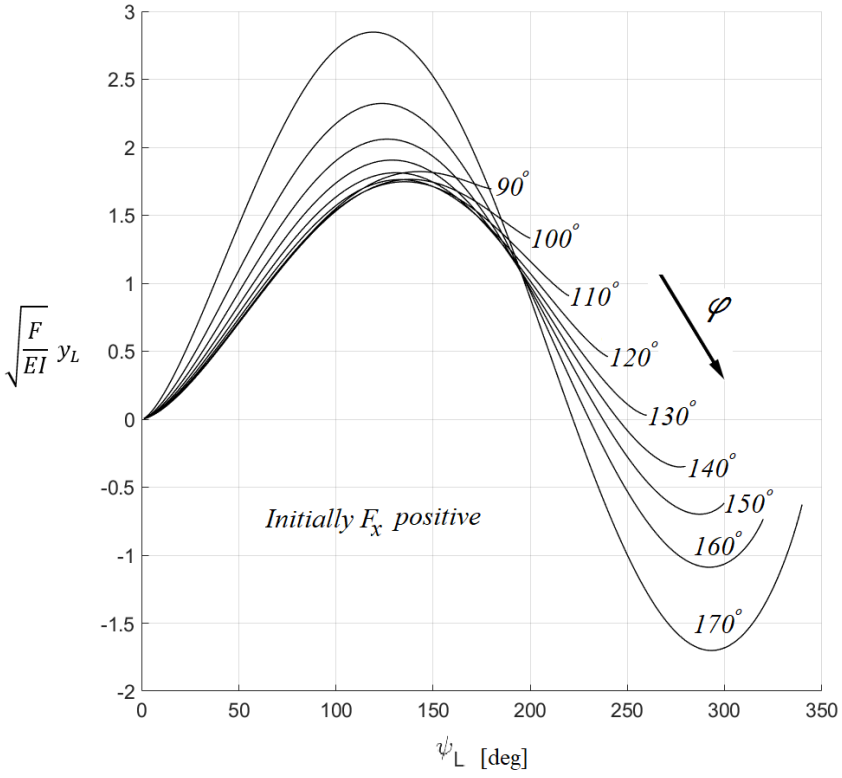

Fig. 10 (c) Initially F_x positive follower load: dimensionless term $\sqrt{\frac{F}{EI}}y_L$ as function of ψ_L angle and parameter φ

5.5 Extension of the mathematical model to spring-hinged cantilever beam

In the mathematical model exposed in § 3.2 and § 3.3, the clamped end was considered perfect, namely rigid. In this section, the previous mathematical model is extended to the case of a compliant constraint, that is to say a spring-hinged cantilever beam. This problem has already been numerically faced in [29,30], using Runge-Kutta method. This extension offers the opportunity to demonstrate how even more complex problems can be solved through the present analytical method. Being r_T the torsional rigidity of the end spring and ψ_0 the angle at curvilinear abscissa $s = 0$; remark that if and only if $r_T \to \infty$, $\psi_0 \to 0$. Performing the steps of section 3.2 related to F_x negative configuration, observing that in this case $\psi_0 \neq 0$, it is straightforward to get:

$$\eta(\psi) = \sqrt{\frac{2EI}{F}}\left[\sqrt{\cos(\psi_0 + \alpha) - a_1} - \sqrt{\cos(\psi + \alpha) - a_1}\right]$$

$$\xi(\psi) = \sqrt{\frac{EI}{2F}}\left[sin(\psi + \alpha)\ {}^{\frac{1}{2}}_{0}\mathrm{I}\left(\begin{matrix}\frac{1}{4},\frac{1}{2},\frac{1}{2}\\ \\ \frac{1}{4},\frac{3}{2}\end{matrix}\ ;\ a_1, sin^2(\psi + \alpha)\right) + \right.$$

$$\left. -sin(\psi_0 + \alpha)\ {}^{\frac{1}{2}}_{0}\mathrm{I}\left(\begin{matrix}\frac{1}{4},\frac{1}{2},\frac{1}{2}\\ \\ \frac{1}{4},\frac{3}{2}\end{matrix}\ ;\ a_1, sin^2(\psi_0 + \alpha)\right)\right]$$

$$L = \sqrt{\frac{EI}{2F}}\left[sin(\psi_L + \alpha)\ {}^{\frac{1}{2}}_{0}\mathrm{I}\left(\begin{matrix}\frac{3}{4},\frac{1}{2},\frac{1}{2}\\ \\ \frac{3}{4},\frac{3}{2}\end{matrix}\ ;\ a_1, sin^2(\psi_L + \alpha)\right) + \right.$$

$$\left. -sin(\psi_0 + \alpha)\ {}^{\frac{1}{2}}_{0}\mathrm{I}\left(\begin{matrix}\frac{3}{4},\frac{1}{2},\frac{1}{2}\\ \\ \frac{3}{4},\frac{3}{2}\end{matrix}\ ;\ a_1, sin^2(\psi_0 + \alpha)\right)\right]$$

The tricky situation in this case is that there are two angular unknowns; again the final angle ψ_L, which is derived from the previous congruency equation of length invariance, but in this equation it also appears the unknown ψ_0. There is the need to find another equation to resolve this system. The sought equation is given by the rotational equilibrium at the clamped point, where the spring is present. Using the moment-curvature relationship (2), the curvature eq. (6) evaluated in a locked point $s = 0$ and assuming that the moment-deformation relationship of spring is linear, we get:

$$EI\left\{\sqrt{\frac{2F}{EI}\left[cos(\psi_0+\alpha)-\cos(\psi_L+\alpha)\right]+\left(k_{in}+\frac{M}{EI}\right)^2}-k_{in}\right\}=-r_T\,\psi_0$$

Whence, it is easily to obtain:

$$\psi_L = acos\left\{cos(\psi_0+\alpha)-\frac{EI}{2F}\left[\left(k_{in}-\frac{r_T}{EI}\,\psi_0\right)^2-\left(k_{in}+\frac{M}{EI}\right)^2\right]\right\}-\alpha$$

The problem is therefore analytically complete. Moreover, if this last relation is replaced in the length inextensible equation, the two unknowns appear to be decoupled, thus the solution complexity stays in a one-dimensional problem.

Repeating the steps already well known, the solution for the F_x positive configuration is obtained:

$$\xi(\psi)=\sqrt{\frac{2EI}{F}}\left[\sqrt{\cos(\psi_0+\alpha)+a_2}-\sqrt{\cos(\psi+\alpha)+a_2}\right]$$

$$\eta(\psi)=\sqrt{\frac{EI}{2F}}\frac{1}{\sqrt{a_2}}\left[\sin(\psi_0+\alpha)^{-\frac{1}{2}}\,\mathrm{I}_{-\beta}\left(\begin{matrix}\beta,\frac{1}{2},\frac{1}{2}\\ \\ \beta,\frac{3}{2}\end{matrix};\frac{1}{a_2},sin^2(\psi_0+\alpha)\right)\right.$$

$$\left.-sin(\psi+\alpha)^{-\frac{1}{2}}\,\mathrm{I}_{-\beta}\left(\begin{matrix}\beta,\frac{1}{2},\frac{1}{2}\\ \\ \beta,\frac{3}{2}\end{matrix};\frac{1}{a_2},sin^2(\psi+\alpha)\right)\right]$$

$$\forall\,\beta\in\mathbb{R}\backslash\{\mathbb{Z}^-,0\},\ \ n\neq 2j\ \wedge\ j\geq 0$$

$$L = \sqrt{\frac{EI}{2F}}\frac{1}{\sqrt{a_2}}\left[\sin(\psi_0+\alpha)\;{}^{-\frac{1}{2}}_{0}\mathrm{I}\left(\begin{matrix}\frac{1}{2},\frac{1}{2},\frac{1}{2}\\ \\ \frac{1}{2},\frac{3}{2}\end{matrix};\frac{1}{a_2},sin^2(\psi_0+\alpha)\right)\right.$$

$$\left.-sin(\psi_L+\alpha)\;{}^{-\frac{1}{2}}_{0}\mathrm{I}\left(\begin{matrix}\frac{1}{2},\frac{1}{2},\frac{1}{2}\\ \\ \frac{1}{2},\frac{3}{2}\end{matrix};\frac{1}{a_2},sin^2(\psi_L+\alpha)\right)\right]$$

$$n \neq 2j+1 \;\wedge\; j \geq k$$

$$\psi_L = asin\left\{\frac{EI}{2F}\left[\left(k_{in}-\frac{r_T}{EI}\,\psi_0\right)^2-\left(k_{in}+\frac{M}{EI}\right)^2\right]-cos(\psi_0+\alpha)\right\}-\alpha$$

An example is reported in Fig.11, where the geometry and material are the same as § 5.1 and the analytical results are still compared with the finite element method. The torsional spring have rigidity $r_T = 100\ Nm$, and the beam is subjected to a force $F = 15\ N$. In the F_x *negative configuration* the angle values are $\psi_0 = 7.45°$ $\psi_L = 91°$, while in F_x positive configuration these are $\psi_0 = 6.30°$ $\psi_L = 63.25°$.

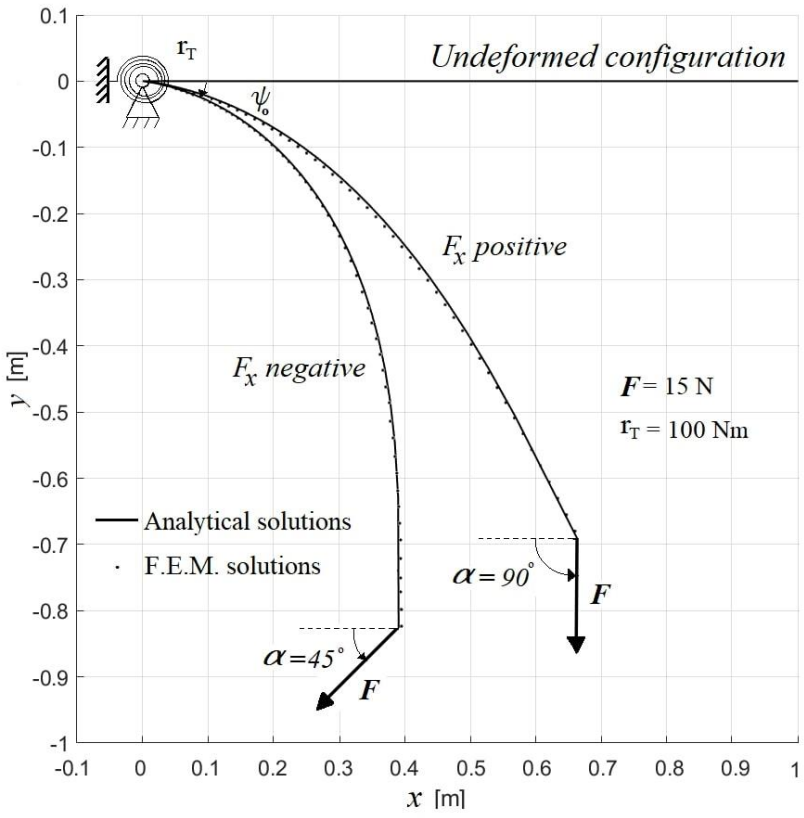

Fig.11. Spring-hinged cantilever beam in F_x negative and F_x positive configurations

5.6 Cantilever beam loaded from a fixed point through an inextensible cable

This last application concerns a particular case, when the beam is deformed constraining the second end through an inextensible cable, locked at a fixed point (Fig.12). This case is widely discussed in [31,32] where the author uses the elliptic integral for his solutions. For this configuration, the magnitude force, the angular direction force α and obviously the end-angle ψ_L are all unknowns; conversely, the length of the beam L, the length L_c of the cable and the coordinates x_c and y_c of the fixed point are established (see Fig.12. for an enhanced clearness).

To reach the uniqueness of the solution, thus obtaining the unknowns F, α, ψ_L , three equations are obviously necessary; one of these is the length conservation (11), while the others two should be searched through geometric congruence of Fig.12. With a simple reasoning, we obtain the geometric relations:

$$|x_L - x_c| = L_c\,|cos(\alpha)|$$

$$|y_L - y_c| = L_c\,|sin(\alpha)|$$

Assigned the values of L, L_c ,x_c y_c, the variables F, α, ψ_L are given by the system of equations composed of the previous geometric equations and the eq. (11). A numerical example is provided in Fig.13, wherein a beam with same geometric and material features of Fig.3 is subjected at three different configurations of cable lengths and hinges positions.

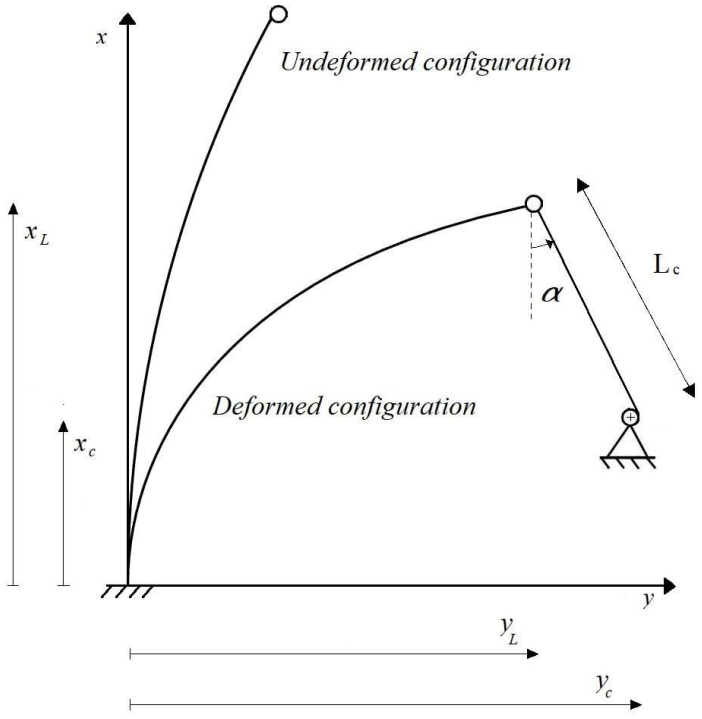

Fig.12. Static scheme of cantilever beam locked to a fixed point by a cable

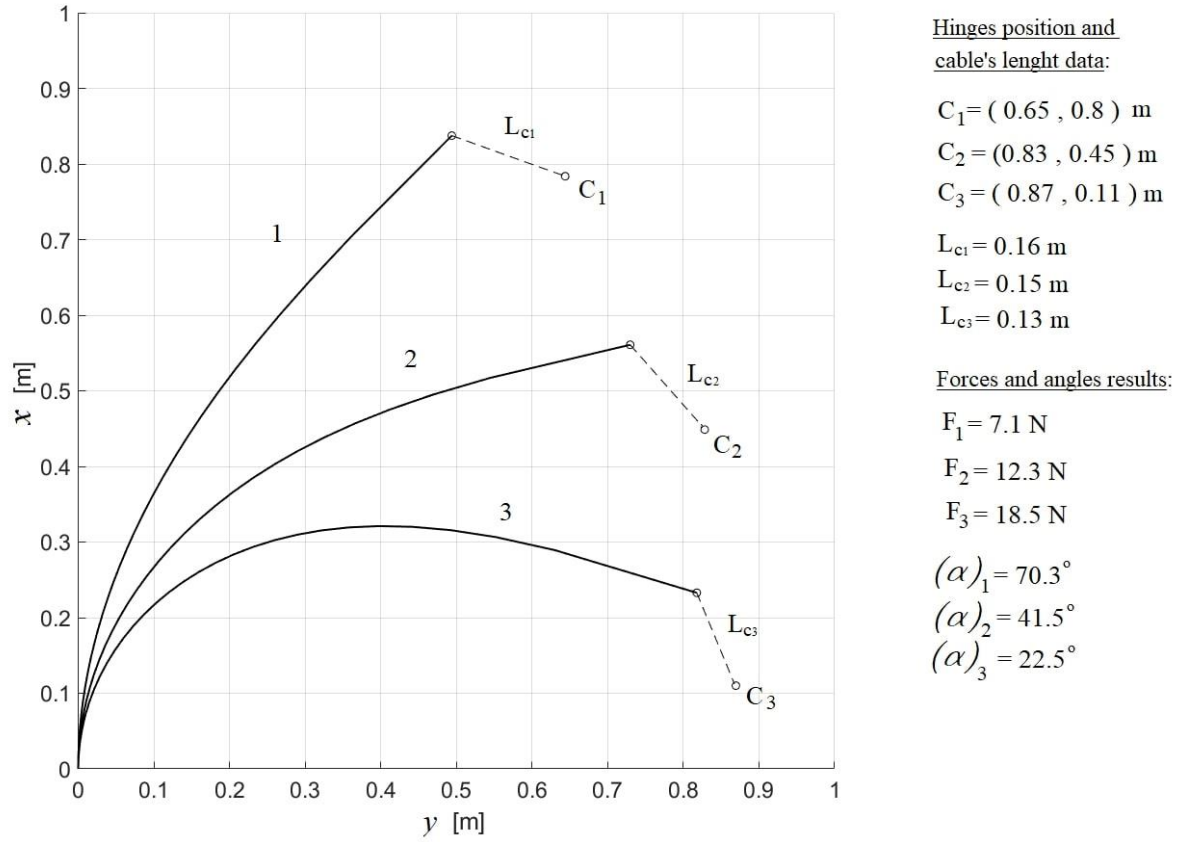

Fig.13. Beam subjected to various configurations of cable length and hinge positions

6. Comparison with the solution based on the series representation of elliptic integrals

The classical elliptic integral solution of a cantilever beam with an inclined load is [7]:

$$x(\psi) = \frac{1}{k}\{\cos(\alpha)\,[F(m,p) - F(n(\psi),p)] + 2[E(n(\psi),p) - E(m,p)]$$

$$+ 2\,p\,sin(\alpha)[\cos(m) - \cos(n(\psi))]\}$$

$$y(\psi) = \frac{1}{k}\{2\,p\cos(\alpha)\,[\cos(m) - \cos(n(\psi))] - \sin(\alpha)[F(m,p) - F(n(\psi),p)]$$

$$+ 2[E(n(\psi),p) - E(m,p)]\}$$

$$L = \frac{1}{k}[K(p(\psi_L)) - F(m,p(\psi_L))]$$

Where:

$$k = \sqrt{\frac{F}{EI}} \quad ; \quad p = sin\left(\frac{\psi_L + \alpha}{2}\right) \quad ; \quad m = sin^{-1}\left[\frac{\sin\left(\frac{\alpha}{2}\right)}{p}\right] \quad ; \quad n = sin^{-1}\left[\frac{sin(\psi + \alpha)}{2}\right]$$

and

$$F(\phi,q)=\int_0^{\phi}\frac{d\phi}{\sqrt{1-q^2\,sin^2(\phi)}}=\sin(\phi)\sum_{n=0}^{\infty}\sum_{k=0}^{\infty}\frac{\left(\frac{1}{2}\right)_{n+k}\left(\frac{1}{2}\right)_n\left(\frac{1}{2}\right)_k}{\left(\frac{3}{2}\right)_{n+k}}\frac{[q^2\,sin^2(\phi)]^n}{n!}\frac{[sin^2(\phi)]^k}{k!}$$

$$E(\phi,q)=\int_0^{\phi}\sqrt{1-q^2\,sin^2(\phi)}\;d\phi=\sin(\phi)\sum_{n=0}^{\infty}\sum_{k=0}^{\infty}\frac{\left(\frac{1}{2}\right)_{n+k}\left(-\frac{1}{2}\right)_n\left(\frac{1}{2}\right)_k}{\left(\frac{3}{2}\right)_{n+k}}\frac{[q^2\,sin^2(\phi)]^n}{n!}\frac{[sin^2(\phi)]^k}{k!}$$

$$K(q)=F\left(\frac{\pi}{2},q\right)=\frac{\pi}{2}\sum_{n=0}^{\infty}\frac{\left(\frac{1}{2}\right)_n\left(\frac{1}{2}\right)_n}{(1)_n}\frac{(q^2)^n}{n!}$$

are the incomplete elliptic integrals of first and second order and the complete elliptic integral of first order. On the left is their Legendre normal form, on the right their analytical representations by means of hypergeometric series [23]. The analytical representation provides a measure of the computational complexity required for the numerical calculation of elliptic integrals, as already discussed in the introduction. Thus, it is now possible to get an analytical comparison between the solution through elliptic integrals and the solution previously discussed. The displacements $x(\psi)$ and $y(\psi)$ with elliptic integrals need four double hypergeometric series calculation; otherwise, the method here presented only involves two hypergeometric double series , eq.s (10 or 14); otherwise. The advantage for the computation of (ψ) , $y(\psi)$ is therefore evident.

For the length conservation equation, developing the previous relations concerning elliptic integrals one obtains :

$$\sqrt{\frac{F}{EI}}\,L=\frac{\pi}{2}\sum_{n=0}^{\infty}\frac{\left(\frac{1}{2}\right)_n\left(\frac{1}{2}\right)_n}{(1)_n}\frac{\left[sin^2\left(\frac{\psi_L+\alpha}{2}\right)\right]^n}{n!}+$$

$$-\frac{\sin\left(\frac{\alpha}{2}\right)}{sin\left(\frac{\psi_L+\alpha}{2}\right)}\sum_{n=0}^{\infty}\sum_{k=0}^{\infty}\frac{\left(\frac{1}{2}\right)_{n+k}\left(\frac{1}{2}\right)_n\left(\frac{1}{2}\right)_k}{\left(\frac{3}{2}\right)_{n+k}}\frac{\left[sin^2\left(\frac{\alpha}{2}\right)\right]^n}{n!}\frac{\left[\frac{sin^2\left(\frac{\alpha}{2}\right)}{sin^2\left(\frac{\psi_L+\alpha}{2}\right)}\right]^k}{k!}$$

The advantage regarding the calculation of length conservation concerns only a double series, eq. (11) as compared to a double plus a single series as above. However, it is required to iterate several time the length

conservation to get the value of ψ_L. Therefore, its impact on the overall time cost is more severe than computation of coordinates.

Table 2 concerns the comparison between the speed of convergence of the two approaches. The bisection method was used to solve the implicit equation, the value of dimensionless parameter is $\sqrt{\frac{F}{EI}}\, L = 1.2665$ and the angle direction of inclined load is α=45°. For both computations the convergence criterion is the same already set in § 4, and the tolerance value is 10^{-4}.

Concerning the reliability of our method, besides the validations already performed with our numerical solutions, in Tab. 3 the comparison is extended to values computed by other authors for conservative and non-conservative load (follower load), using their own numerical approach. It is interesting to highlight that all computed values coluld also be obtained by the diagrams in Fig. 5 and 6 (a, b, c).

Table 2 Comparison of speed convergence between the proposed hypergeometric method and the elliptical method in series representation

	ψ_L [°]	Number of iterations	Total number of calculated series terms	Computational time ratio
Proposed method	44.9955	7	409	$\frac{t_{P.M.}}{t_{E.M.}} = 0.2651$
Elliptical method in series representation	45.0051	13	942	P.M.= Proposed method E.M.= Elliptical method in series representation

Table 3 Comparison between some results obtained from other authors for conservative and non-conservative load

Conservative load

Reference	$\sqrt{\frac{F}{EI}}\,L$	α [°]	ψ_L [°]	$\frac{x_L}{L}$	$\frac{y_L}{L}$	Proposed method		
						ψ_L [°]	$\frac{x_L}{L}$	$\frac{y_L}{L}$
Belendez et al. (2002)-[33] (Numerical integration)	1.2124	90	36.0900	0.8953	0.4053	35.9767	0.8950	0.4049
Batista (2014)- [12] (Elliptic functions)	1	90	28.4121	0.9356	0.3206	28.4273	0.9389	0.3256
Wang et al. (1992)- [34] (Runge-Kutta numerical method)	$\sqrt{3}$	45	77.7733	0.5572	0.7330	77.7729	0.5572	0.7329
	$\sqrt{3}$	135	29.2758	0.9274	0.3439	29.2650	0.9275	0.3439

Non Conservative load

Reference	$\sqrt{\frac{F}{EI}}\,L$	φ [°]	ψ_L [°]	$\frac{x_L}{L}$	$\frac{y_L}{L}$	Proposed method		
						ψ_L [°]	$\frac{x_L}{L}$	$\frac{y_L}{L}$
Shvartsman (2007) - [28] (Runge-Kutta numerical method)	2	90	101.7800	0.3428	0.7862	101.7787	0.3427	0.7861
Mutyalarao et al. (2010)- [15] (Runge-Kutta numerical method)	$\sqrt{2.175}$	90	60	0.7313	0.6080	59.9812	0.7313	0.6080

Conclusions

The present paper discusses a new closed-form solution of slender beams submitted to planar large displacements. The hypotheses introduced regard the linear elastic behaviour of the material, the invariance of the section moment of inertia, the inconsistency of axial and shear deformations by respect to bending. The beams considered present a constant initial curvature, including straight lines. The solution is valid if the radius of curvature of the beam in the displaced configuration has an unchanging sign.

The analytical solution makes use of a new hypergeometric function of two variables. Therefore, the solution is gained through a series of functions; although, the same can be developed in integral form, in terms of complete or simplified formulation, as developed in the Appendix. The series uniform convergence is guaranteed for a convex region whose existence is demonstrated.

By respect to the elliptic integral approach, the present one has a lower numerical cost. In fact, the solution involves the computation of a lower number of terms in the series. Similar reductions appear adopting the numerical integration approach, as developed in the Appendix; the integral representation of the hypergeometric functions only requires compute two integrals instead of four with elliptic integrals.

The solution process is detailed for the classical end-loaded cantilever beam. However, some simple artifices allow extending the procedure to encompass some addition configurations:

1. Hinged-roller supported beam subjected to compressive load
2. Cantilever beam subjected to end-follower load
3. Spring-hinged end-loaded cantilever beam
4. Cantilever beam loaded from a fixed point through an inextensible cable.

Technical design curves for straight cantilever beams with end and follower loads are provided. These diagrams are given in adimensional form, so that they offer immediate results for any load (in terms of

magnitude and direction) applied to the beam end. The results given concern the end-point rotation and displacements in the *x* and *y* directions.

Appendix

Before demonstrating the integral representation of the new two variables hypergeometric series, it is useful to find the integral representation of the one variable hypergeometric series $\mathrm{I}^{*}_{\gamma}\left(\begin{matrix}a\,,b\\ c\end{matrix};x\right)$ that can be defined as a generalization of the Gauss hypergeometric function ${}_2F_1(a,b\,;c\,;x)$:

$$\mathrm{I}^{*}_{\gamma}\left(\begin{matrix}a\,,b\\ c\end{matrix};x\right)=\sum_{n=0}^{\infty}\frac{(a)_{\gamma n}(b)_n}{(c)_{\gamma n}}\,\frac{x^n}{n!}$$

Using the property 1), the ratio of Pochhammer coefficients *a* and *c* is expressed as:

$$\frac{(a)_{\gamma n}}{(c)_{\gamma n}}=\frac{\Gamma(c)}{\Gamma(a)\Gamma(c-a)}\,\frac{\Gamma(a+\gamma n)\Gamma(c-a)}{\Gamma(c+\gamma n)}=\frac{\Gamma(c)}{\Gamma(a)\Gamma(c-a)}\,B(a+\gamma n\,,c-a)\qquad\text{(A1)}$$

Where $B(a\,,b)$ is the *Euler Beta function*, given by:

$$B(a\,,b)=\int_0^1 t^{a-1}(1-t)^{b-1}\,dt=\frac{\Gamma(a)\,\Gamma(b)}{\Gamma(a+b)}$$

Using the latter definition and (A1) one obtains:

$$\mathrm{I}^{*}_{\gamma}\left(\begin{matrix}a\,,b\\ c\end{matrix};x\right)=\frac{\Gamma(c)}{\Gamma(a)\Gamma(c-a)}\sum_{n=0}^{\infty}(b)_n\,\frac{x^n}{n!}\int_0^1 t^{a+\gamma n-1}(1-t)^{c-a-1}\,dt=$$

$$=\frac{\Gamma(c)}{\Gamma(a)\Gamma(c-a)}\int_0^1 t^{a-1}(1-t)^{c-a-1}\left(\sum_{n=0}^{\infty}(b)_n\,\frac{(t^{\gamma}\,x)^n}{n!}\right)dt$$

Applying property {9}:

$$\mathrm{I}^{*}_{\gamma}\left(\begin{matrix}a\,,b\\ c\end{matrix};x\right)=\frac{\Gamma(c)}{\Gamma(a)\Gamma(c-a)}\int_0^1 t^{a-1}(1-t)^{c-a-1}\,(1-xt^{\gamma})^{-b}dt\qquad(A2)$$

The developments of the two variables hypergeometric function is more articulated than the previous one, but indeed similar. It is supposed that $c_1 \neq a \ , \ c_2 \neq b_2$

$$ {}^{\gamma}_{\beta}\mathrm{I}\left(\begin{matrix} a\ ,\ b_1\ ,b_2 \\ c_1\ ,c_2 \end{matrix}\ ;\ x,y\right) = \sum_{n=0}^{\infty}\sum_{k=0}^{\infty} \frac{(a)_{\beta+\gamma n+k}\,(b_1)_n\,(b_2)_k}{(c_1)_{\beta+\gamma n}\,(c_2)_k}\,\frac{x^n\,y^k}{n!\,k!} $$

Using the same steps of (A1)

$$ \frac{(b_2)_k}{(c_2)_k} = \frac{\Gamma(c_2)}{\Gamma(b_2)\Gamma(c_2-b_2)}\,B(b_2+k\,,c_2-b_2) $$

and applying the property 1)

$$ \frac{(a)_{\beta+\gamma n+k}}{(c)_{\beta+\gamma n}} = \frac{\Gamma(a+\beta)\,\Gamma(c_1)}{\Gamma(a)\,\Gamma(c_1+\beta)}\,\frac{(a+\beta)_{\gamma n}\,(a+\beta+\gamma n)_k}{(c_1+\beta)_{\gamma n}} $$

Whence:

$$ {}^{\gamma}_{\beta}\mathrm{I}\left(\begin{matrix} a\ ,\ b_1\ ,b_2 \\ c_1\ ,c_2 \end{matrix}\ ;\ x,y\right) = $$

$$ = \frac{\Gamma(c_1)\Gamma(c_2)\Gamma(a+\beta)}{\Gamma(a)\,\Gamma(b_2)\,\Gamma(c_1+\beta)\Gamma(c_2-b_2)}\sum_{n=0}^{\infty}\sum_{k=0}^{\infty}\frac{(a+\beta)_{\gamma n}\,(a+\beta+\gamma n)_k\,(b_1)_n}{(c_1+\beta)_{\gamma n}}\,\frac{x^n\,y^k}{n!\,k!}\int_0^1 t^{b_2+k-1}(1-t)^{c_2-b_2-1}\,dt = $$

$$ = \frac{\Gamma(c_1)\Gamma(c_2)\Gamma(a+\beta)}{\Gamma(a)\,\Gamma(b_2)\Gamma(c_1+\beta)\ \Gamma(c_2-b_2)}\sum_{n=0}^{\infty}\frac{(a+\beta)_{\gamma n}\ (b_1)_n}{(c_1+\beta)_{\gamma n}}\,\frac{x^n}{n!}\int_0^1 t^{b_2+k-1}(1-t)^{c_2-b_2-1}\left(\sum_{k=0}^{\infty}(a+\beta+\gamma n)_k\frac{(ty)^k}{k!}\right)dt \overset{\{9\}}{=} $$

$$ = \frac{\Gamma(c_1)\Gamma(c_2)\Gamma(a+\beta)}{\Gamma(a)\Gamma(b_2)\Gamma(c_1+\beta)\,\Gamma(c_2-b_2)}\sum_{n=0}^{\infty}\frac{(a+\beta)_{\gamma n}\ (b_1)_n}{(c_1+\beta)_{\gamma n}}\,\frac{x^n}{n!}\int_0^1 t^{b_2+k-1}(1-t)^{c_2-b_2-1}(1-yt)^{-a-\beta-\gamma n}\,dt \overset{\{9\}}{=} \qquad (A3) $$

$$ = \frac{\Gamma(c_1)\Gamma(c_2)\Gamma(a+\beta)}{\Gamma(a)\,\Gamma(b_2)\,\Gamma(c_1+\beta)\Gamma(c_2-b_2)}\int_0^1 t^{b_2+k-1}(1-t)^{c_2-b_2-1}(1-yt)^{-a-\beta}\left(\sum_{n=0}^{\infty}\frac{(a+\beta)_{\gamma n}\ (b_1)_n}{(c_1+\beta)_{\gamma n}}\,\frac{\left[\frac{x}{(1-yt)^{\gamma}}\right]^n}{n!}\right)dt $$

Applying the integral representation as in eq. (A2), one finally obtains:

$$\underset{\beta}{\overset{\gamma}{\mathrm{I}}}\left(\begin{matrix} a\ ,\ b_1\ ,b_2 \\ c_1\ ,c_2 \end{matrix}\ ;\ x,y\right)=$$

$$=\frac{\Gamma(c_1)\,\Gamma(c_2)}{\Gamma(a)\,\Gamma(b_2)\,\Gamma(c_1-a)\,\Gamma(c_2-b_2)}\int_0^1\int_0^1 t^{b_2-1}\,(1-t)^{c_2-b_2-1}\,u^{a+\beta-1}(1-u)^{c_1-a-1}(1-yt)^{-a-\beta}\left[1-x\left(\frac{u}{1-yt}\right)^{\gamma}\right]^{-b_1}du\,dt$$

If, as it happens in the previously discussed solutions, $c_1=a$, the latter integral representation is no more valid. From (A3) it is however easy to get the integral representation for this case:

$$\underset{\beta}{\overset{\gamma}{\mathrm{I}}}\left(\begin{matrix} a\ ,\ b_1\ ,b_2 \\ c_1\ ,c_2 \end{matrix}\ ;\ x,y\right)=\frac{\Gamma(c_2)}{\Gamma(b_2)\Gamma(c_2-b_2)}\int_0^1 t^{b_2-1}\,(1-t)^{c_2-b_2-1}(1-yt)^{-a-\beta}\left[1-\frac{x}{(1-yt)^{\gamma}}\right]^{-b_1}dt$$

REFERENCES

[1] Todhunter I.,1886, A History of the Theory of Elasticity and of the Strength of Materials vol.1. Cambridge University Press.

[2] Truesdell C., 1960. The Rational Mechanics of Flexible or Elastic Bodies: 1638–1788. Leonhard Euler. Opera Omnia. Birkhauser.

[3] Lagrange J.L., 1868. Sur la figure des colonnes, in: Ouevres de Lagrange (Publ. de M.J.A. Serret) vol.2. Paris, Gauthier-Villars.

[4] Saalschütz L., 1880. Der belastete Stab unter Einwirkung einer seitlichen Kraft. B. G. Teubner. Leipzig.

[5] Levien R., 2008. The elastica: a mathematical history. University of California at Berkeley.

[6] Goss V.G.A., 2009. The history of the planar Elastica: insights into mechanics and scientific method. Sci. Educ. 18 (8), 1057–1082.

[7] Frish-Fay R., 1962. Flexible bars, Butterworths. London.

[8] Barten H.J., 1944. On the deflection of a Cantilever Beam. Quarterly of Applied Mathematics, 2, 168-171.

[9] Bisshop K.E., 1945. Drucker D.C., Large deflection of cantilever beams. Quarterly of Applied Mathematics 3 ,272–275.

[10] De Bona F., Zelenika S., 1997. A generalized elastica-type approach to the analysis of large displacements of spring-strips. Proceedings of the Institution of Mechanical Engineers, Part C: Journal of Mechanical Engineering Science.

[11] Chen L., 2010. An integral approach for large deflection cantilever beams. International Journal of Non-Linear Mechanics 45 301–305.

[12] Batista M., 2014. Analytical treatment of equilibrium configurations of cantilever under terminal loads using Jacobi elliptical functions. International Journal of Solids and Structures 51, 2308–2326.

[13] Banerjee A., Bhattacharya B., Mallik A.K., 2008. Large deflection of cantilever beams with geometric nom-linearity: Analytical and numerical approaches. International Journal of Non-Linear Mechanics 43, 366-376.

[14] Nallathambi A.K., Rao C.L., Srinivasan S.M., 2010. Large deflection of constant curvature cantilever beam under follower load. International Journal of Mechanical Science 52, 440-445.

[15] Mutyalarao M., Bharathi D., Nageswara Rao B., 2010. Large deflections of a cantilever beam under an inclined end load. Applied Mathematics and Computation 217, 3607-3613.

[16] Tari H., 2013. On the parametric large deflection study of Euler-Bernoulli cantilever beams subjected to combined tip point loading. International Journal of Non-Linear Mechanics 49 90-99.

[17] Johansson F., 2019. Numerical Evaluation of Elliptic Functions, Elliptic Integrals and Modular Forms. Elliptic Integrals, Elliptic Functions and Modular Forms in Quantum Field Theory. Springer,Switzerland.

[18] Fukushima T., 2012. Series expansions of symmetric elliptic integrals. Mathematics of Computation, vol. 81, no.278, 957–990.

[19] Bailey D.H., Borwein J.M.,2011. High-precision numerical integration: Progress and challenges. Journal of Symbolic Computation ,46 , 741–754.

[20] Reissner E., 1972. On one-dimensional finite-strain beam theory: the plane problem. Journal of Applied Mathematics and Physics (ZAMP) 23 795-804.

[21] Goto Y., Yoshimitsu T., Obata M., 1990. Elliptic integral solutions of plane elastica with axial and shear deformations. International Journal of Solids Structures vol.26 No. 4 375-390.

[22] Ahuett-Gaza H., Chaides O., Garcia P.N., Urbina P., 2014. Studies about the use of semicircular beams as hinges in large deflection planar compliant mechanisms. Precision Engineering 38 711–727.

[23] Changizi M. A., Abolfathi A., Stiharu I., 2015. Mems Wind Speed Sensor: Large deflection of curved micro-cantilever beam under uniform horizontal force. Proceedings of the ASME 2015 International Mechanical Engineering Congress and Exposition IMECE2015, Houston, Texas.

[24] Levy O., Krylov S., Goldfarb I., 2006.Design considerations for negative Poisson ratio structures under large deflection for MEMS applications. Smart Materials Structures 15 1459–1466.

[25] Iandiorio C., Salvini P., 2018. An Analytical Solution for Large Displacements of End-Loaded Beams. Proceedings of the 1st International Conference on Numerical Modelling in Engineering vol. 2, 320-338, Ghent University.

[26] Cvijovic D., Klinowski J., 1994. On the Integration of Incomplete Elliptic Integrals. Proceedings: Mathematical and Physical Sciences vol. 444 No. 1922 525-532, Royal Society.

[27] Erdélyi A., Bateman H., 1953. Higher Transcendental Functions vol. 1. Bateman Project. McGraw-Hill, New York.

[28] Shvartsman B. S. , 2007. Large deflections of a cantilever beam subjected to a follower force. Journal of Sound and Vibration,vol. 304, 969-973.

[29] Shvartsman B.S.,2013. Analysis of large deflections of a curved cantilever subjected to a tip-concentrated follower force. International Journal of Non-Linear Mechanics, 50, 75-80.

[30] Nageswara Rao B., Nagesh Babu G.L., Venkateswara Rao G., 1987. Large Deflection Analysis of a Spring Hinged Cantilever Beam Subjected to a Tip Concentrated Rotational Load. ZAMM, 67 ,519-520

[31] Dar Yau J., 2010. Closed-form solutions of large deflection for a guyed cantilever column pulled by an inclination cable. Journal of Marine Science and Technology, vol.18, no.1, 130-136.

[32] Batista M., 2015. Large deflection of cantilever rod pulled by cable. Applied Mathematical Modelling 39 , 3175–3182.

[33] Beléndez T., Neipp C., Beléndez A., 2002. Large and small deflections of a cantilever beam. European Journal of Physic, vol. 23, 371-379.

[34] Wang C.M., Kitipornchai S., 1992. Shooting-Optimization technique for large deflection analysis of structural members. Engineering Structures, vol. , 231-240.